TA7
W34m
no. S-77-23
Cop. 2
US-CE-C Property of the United States Government
REFERENCE

MISCELLANEOUS PAPER S-77-23

NUMERICAL ANALYSES OF PENETRATION DYNAMICS IN SUPPORT OF INVESTIGATIONS OF SCALING RELATIONS FOR EARTH PENETRATORS

by

Mark H. Wagner, Christopher C. Fulton

California Research and Technology, Inc.
6269 Variel Avenue, Suite 200
Woodland Hills, Calif. 91367

November 1977
Final Report

Approved For Public Release; Distribution Unlimited

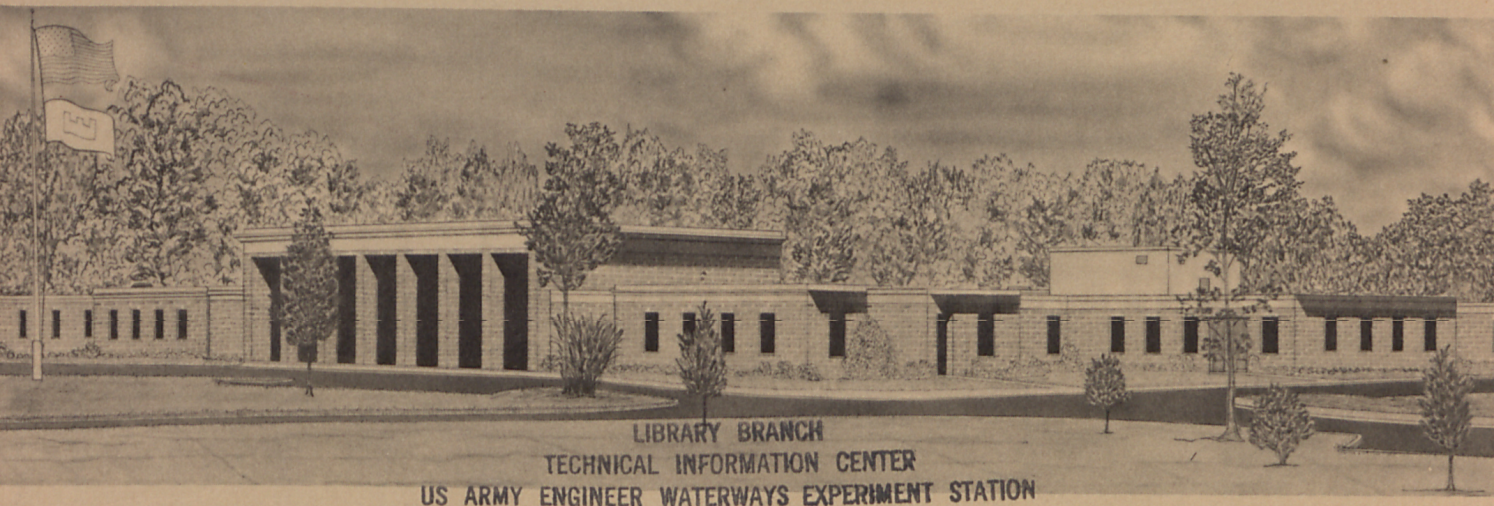

LIBRARY BRANCH
TECHNICAL INFORMATION CENTER
US ARMY ENGINEER WATERWAYS EXPERIMENT STATION
VICKSBURG, MISSISSIPPI

Prepared for Office, Chief of Engineers, U. S. Army
Washington, D. C. 20314

Under Project 4A161102AT22, Task A2, Work Unit 006

Monitored by Soils and Pavements Laboratory
U. S. Army Engineer Waterways Experiment Station
P. O. Box 631, Vicksburg, Miss. 39180

Unclassified

SECURITY CLASSIFICATION OF THIS PAGE *(When Data Entered)*

REPORT DOCUMENTATION PAGE

READ INSTRUCTIONS BEFORE COMPLETING FORM

1. REPORT NUMBER: Miscellaneous Paper S-77-23	2. GOVT ACCESSION NO.
3. RECIPIENT'S CATALOG NUMBER	
4. TITLE *(and Subtitle)*: NUMERICAL ANALYSES OF PENETRATION DYNAMICS IN SUPPORT OF INVESTIGATIONS OF SCALING RELATIONS FOR EARTH PENETRATORS	5. TYPE OF REPORT & PERIOD COVERED: Final report
	6. PERFORMING ORG. REPORT NUMBER
7. AUTHOR(s): Mark H. Wagner Christopher C. Fulton	8. CONTRACT OR GRANT NUMBER(s): DACA 39-77-M-0136
9. PERFORMING ORGANIZATION NAME AND ADDRESS: California Research and Technology, Inc. 6269 Variel Avenue, Suite 200 Woodland Hills, Calif. 91367	10. PROGRAM ELEMENT, PROJECT, TASK AREA & WORK UNIT NUMBERS: Project 4A161102AT22, Task A2 Work Unit 006
11. CONTROLLING OFFICE NAME AND ADDRESS: Office, Chief of Engineers, U. S. Army Washington, D. C. 20314	12. REPORT DATE: November 1977 13. NUMBER OF PAGES: 34
14. MONITORING AGENCY NAME & ADDRESS *(if different from Controlling Office)*: U. S. Army Engineer Waterways Experiment Station Soils and Pavements Laboratory Vicksburg, Miss. 39180	15. SECURITY CLASS. *(of this report)*: Unclassified 15a. DECLASSIFICATION/DOWNGRADING SCHEDULE

16. DISTRIBUTION STATEMENT *(of this Report)*

Approved for public release; distribution unlimited.

17. DISTRIBUTION STATEMENT *(of the abstract entered in Block 20, if different from Report)*

18. SUPPLEMENTARY NOTES

19. KEY WORDS *(Continue on reverse side if necessary and identify by block number)*

Earth penetrators
Finite difference method
Numerical analysis
Penetration
Projectile penetration
Soil penetration

20. ABSTRACT *(Continue on reverse side if necessary and identify by block number)*

Two finite-difference WAVE-L code solutions of projectile penetration have been conducted to assess the effect of projectile sectional pressure (W/A) on penetration dynamics. The results are being used in an investigation of penetration scaling relations underway at the Waterways Experiment Station. The penetrator problems consisted of the normal impacts of rigid-body projectiles into sand targets at a velocity of 200 ft/sec. The projectiles

(Continued)

DD FORM 1 JAN 73 1473 EDITION OF 1 NOV 65 IS OBSOLETE

Unclassified

SECURITY CLASSIFICATION OF THIS PAGE *(When Data Entered)*

20. ABSTRACT (Continued).

were 6 in. in diameter with a 6-in. long, ogive nose (CRH = 1.25). Two penetrator weights were selected, 141.4 lb (Case 1) and 424.1 lb (Case 2), to give projectile sectional pressures of 5 psi for Case 1 and 15 psi for Case 2.

At impact, the force loadings on the rigid penetrators for the two cases are the same, $F_1 = F_2$, so the ratio of decelerations will be inversely proportional to the penetrator weights, i.e., $a_1/a_2 = W_2/W_1 = 3$. As the penetration proceeds, the velocities will differ, due to the different decelerations, and the ratio of forces, F_2/F_1, or scaled deceleration ratio, a_2W_2/a_1W_1, will depart from unity.

Each penetrator problem was run from initial impact to a penetration depth of 8 in., or 2 in. below full nose embedment. From the solution results, the scaled deceleration ratio, a_2W_2/a_1W_1, was computed as a function of depth of penetration. These results showed that the scaled deceleration ratio oscillated around a value of 1 for about the first half of nose embedment; the ratio then steadily increased to a value of 1.06 at a penetration depth of 8 in. The gradually larger force applied to the heavier projectile (Case 2) is due to its penetration velocity staying higher (due to its lesser deceleration), relative to Case 1.

Detailed results of the numerical solutions, including time histories of the penetration dynamics variables, force loading distributions, and field plots of the target response, are presented in the report.

PREFACE

This report was prepared by Messrs. Mark H. Wagner and Christopher C. Fulton of California Research and Technology, Inc., Woodland Hills, California, under PO DACA 39-77-M-0136 as a part of ongoing work at the U. S. Army Engineer Waterways Experiment Station (WES), DA Project No. 4A161102AT22, Task A2, Work Unit 006, "Effectiveness of Earth Penetrators in Various Geologic Environments." The principal investigator at California Research and Technology was Mr. Wagner. The programming and computer runs were conducted by Mr. Fulton.

The problems were specified and the work was monitored by Dr. Behzad Rohani of the Soil Dynamics Division (SDD), Soils and Pavements Laboratory (S&PL), WES, under the supervision of Dr. J. G. Jackson, Jr., and the general direction of Mr. James P. Sale, Chief of S&PL.

COL J. L. Cannon, CE, was Commander and Director of WES during the period this work was performed. Mr. F. R. Brown was Technical Director.

CONTENTS

	Page
PREFACE	1
CONVERSION FACTORS, U. S. CUSTOMARY TO METRIC (SI) UNITS OF MEASUREMENT	3
SCOPE	4
PENETRATOR PROBLEM DESCRIPTION	4
COMPUTATIONAL METHOD	4
NUMERICAL SOLUTION RESULTS	5
REFERENCE	6
TABLES 1 and 2	
FIGURES 1-26	

CONVERSION FACTORS, U. S. CUSTOMARY TO METRIC (SI) UNITS OF MEASUREMENT

U. S. customary units of measurement can be converted to metric (SI) units as follows:

Multiply	By	To Obtain
feet per second	0.3048	metres per second
inches	25.4	millimetres
kips (force)	4.448222	kilonewtons
microns	0.001	millimetres
pounds (mass)	0.4535924	kilograms
pounds (mass) per cubic foot	16.01846	kilograms per cubic metre
pounds (mass) per square foot	4.882428	kilograms per square metre

NUMERICAL ANALYSES OF PENETRATION DYNAMICS IN SUPPORT OF INVESTIGATIONS OF SCALING RELATIONS FOR EARTH PENETRATORS

1. SCOPE

This report describes the results of two finite-difference code calculations of projectile penetration conducted by CRT to provide information of use in the study of penetrator scaling relations. These two calculations were designed specifically to assess the effect of projectile sectional pressure (W/A) on penetration dynamics.

2. PENETRATOR PROBLEM--DESCRIPTION

The penetrator problem considered was the normal impact of a rigid body projectile into a sand target at 200 ft/sec, as shown in Figure 1. The conditions of the two cases considered are listed in Table 1. The projectile for Case 2 weighed 3 times as much as the Case 1 projectile, giving a projectile sectional pressure, W/A, of 5 psi for Case 1 and 15 psi for Case 2; all other conditions of the problems were identical.

The nominal properties of the sand target are listed in Table 2. The material model used was the same as that used for Layer 2 of the Watching Hill Site at DRES in a previous study[1], except that the low-pressure end of the yield surface was modified so that the cohesion would be equal to zero.

The penetrator/target interface was assumed to be frictionless for these problems.

3. COMPUTATIONAL METHOD

Numerical solutions of the penetrator problems were obtained with WAVE-L, a two-dimensional finite-difference Lagrangian hydrodynamic-elastic-plastic code. This code has been employed to solve penetrator problems on a number of DNA and WES projects during the past few years.

The computational grid set up for these problems is partially shown in Figure 2. The basic cell size used in the target was $\Delta r_o = \Delta z_o = 0.5$ in., or 1/6 the projectile radius. Beyond a radius of 6 in. and a depth of 12 in., the cell dimensions were gradually increased, in 2% steps. The overall grid extended to a radius of 30.5 in. and a depth of 36.5 in., comprising 2800 grid points. This grid extends beyond the boundaries of wave propagation that took place during these problems (which were run to a penetration depth of 8 in.), so that they could be restarted and continued to longer times if desired.

The integration time step varies during the course of the problem, depending on the sound speed, minimum cell dimension, and stability criteria selected. For these problems, the average time step was 1.5 μsec.

4. NUMERICAL SOLUTION RESULTS

Each penetrator problem was run from initial impact to a penetration depth of 8 in., or 2 in. below full nose embedment. The computed penetrator deceleration vs depth of penetration for each case is shown in Figure 3. Time histories of the penetrator deceleration, velocity, depth of penetration, and attached length (vertical distance from nose tip to point of separation of projectile from target) are shown in Figure 4. The deceleration for Case 1 is seen to be approximately 3 times that of Case 2, i.e., the decelerations are inversely proportional to the penetrator weights (or W/A). This scaling ratio can be examined in detail from Figure 5, which is a plot of $\frac{a_2(\frac{W}{A})_2}{a_1(\frac{W}{A})_1}$ vs $\frac{\text{penetration depth}}{\text{nose length}}$, where the

subscripts refer to the case number. The scaled deceleration ratio is seen to oscillate around a value of 1 for about the first half of nose embedment; the ratio then steadily increases to a value of 1.06 at a penetration depth of 1-1/3 nose lengths (8 in.). The gradually larger force seen in Case 2 is due to its penetration velocity staying higher, relative to Case 1. At 8 in. penetration depth, the penetration velocities were 191 ft/sec for Case 1 and 197 ft/sec for Case 2.

A series of field plots at penetration depths of 2, 4, 6, and 8 in. were obtained for each case. These plots show the overall projectile and target configuration, the extent of plastic deformation in terms of the generalized plastic strain ($\overline{\varepsilon^P}$), the velocity vectors, and the principal stress field. These plots are presented in Figures 6-13 for Case 1 and Figures 14-21 for Case 2.

Comparative plots of the loadings on the penetrator, i.e., distributions of normal stress, axial force, and radial force, for penetration depths of 2, 4, 6, and 8 in. are shown in Figures 22-25. Finally, a comparison of the loadings for Case 2 at 8 in. depth and for Case 1 at the same penetration velocity as Case 2, i.e., 197 ft/sec, is shown in Figure 26. The penetration depth at which the penetration velocity for Case 1 was at this value (197 ft/sec) was 3.85 in.

REFERENCE

1. M. H. Wagner, K. N. Kreyenhagen, and W. S. Goerke, *Numerical Analysis of DNA Earth Penetrator Experiment at DRES*, DNA Report 3537F, June 1975.

TABLE 1. PENETRATOR PROBLEM CONDITIONS

	Projectile					Target
	Impact Velocity	Weight	Diameter	W/A	Nose	
Case 1	200 ft/sec	64125 gm (141.4 lb)	6 in.	5 psi	1.25 CRH	Sand
Case 2	200 ft/sec	192375 gm (424.1 lb)	6 in.	15 psi	1.25 CRH	Sand

TABLE 2. PROPERTIES OF SAND TARGET

Density, ρ_o	1.4256 gm/cm^3 89 lb/ft^3
Air fraction, V_a	40%
Cohesion	0
Unconfined compressive strength	0
Unconfined tensile strength	0
Mises limit, $Y_{max} = \sqrt{3J'_2}_{max}$	2906 psi
Initial value of:	
Bulk modulus, K_o	3292 psi
Shear modulus, G_o	2469 psi
Constrained modulus, M_o	6585 psi
Young's modulus, E_o	5926 psi
Poisson's ratio, ν_o	0.2
Dilatational velocity, c_o	585 ft/sec

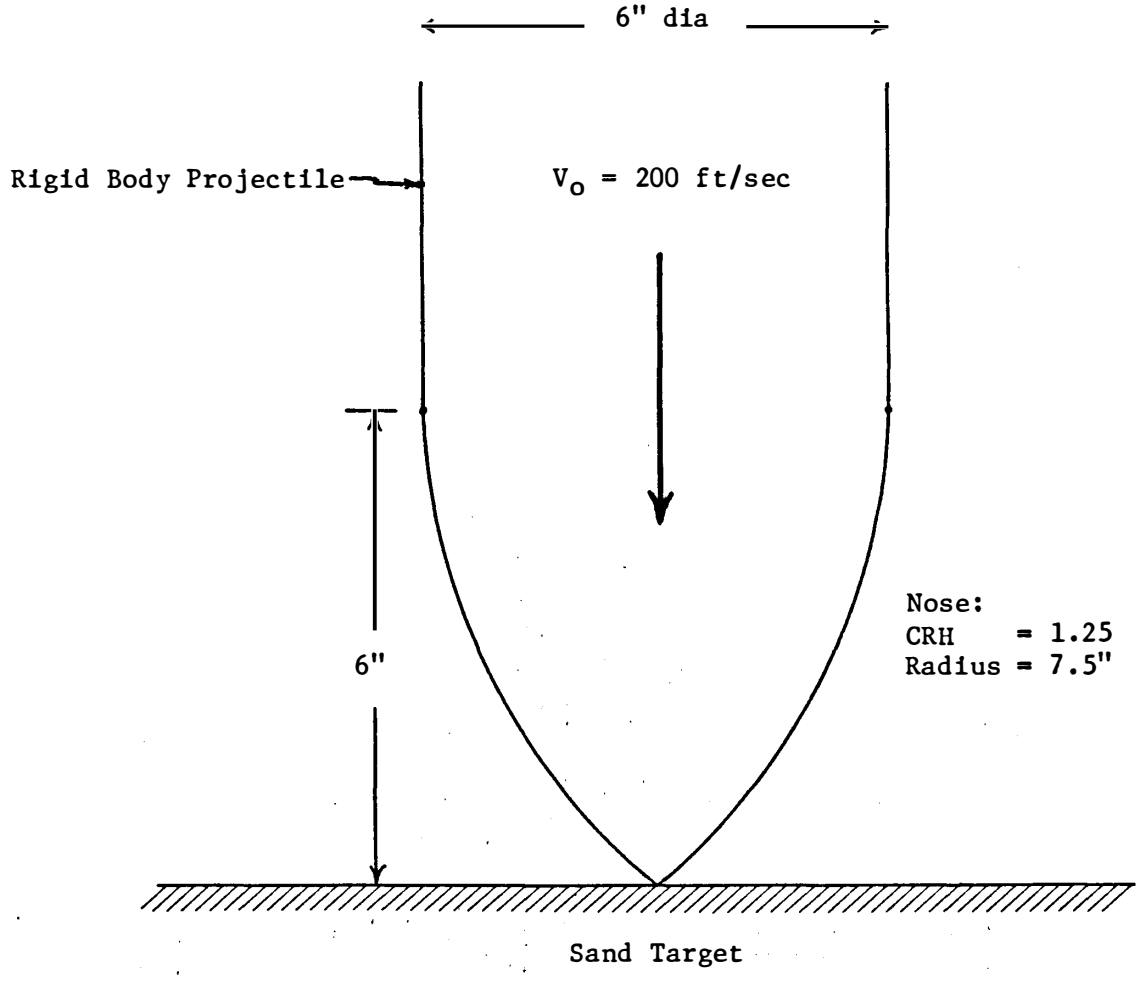

Figure 1. Penetrator Problem Conditions

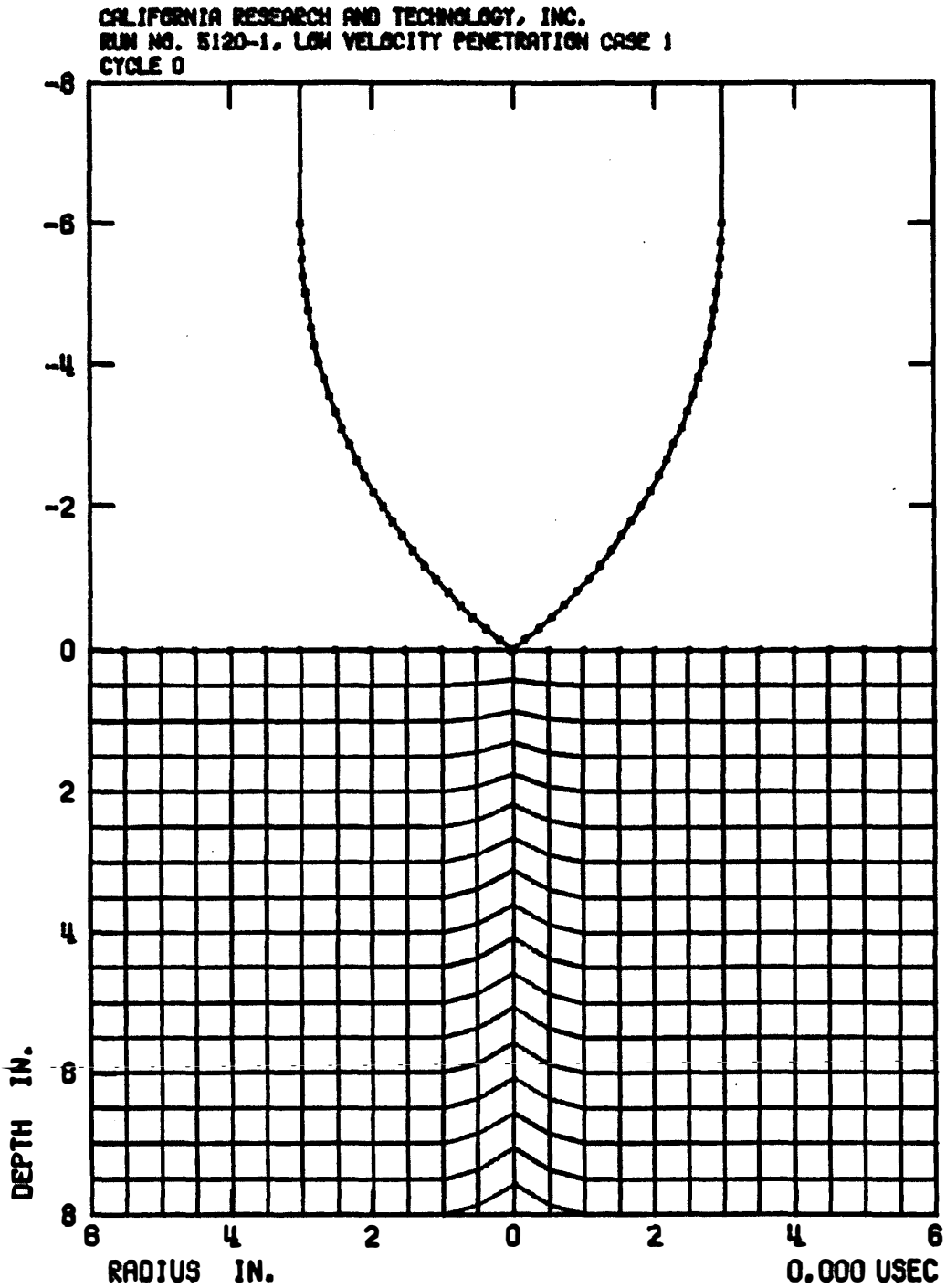

Figure 2. Initial Computational Grid.

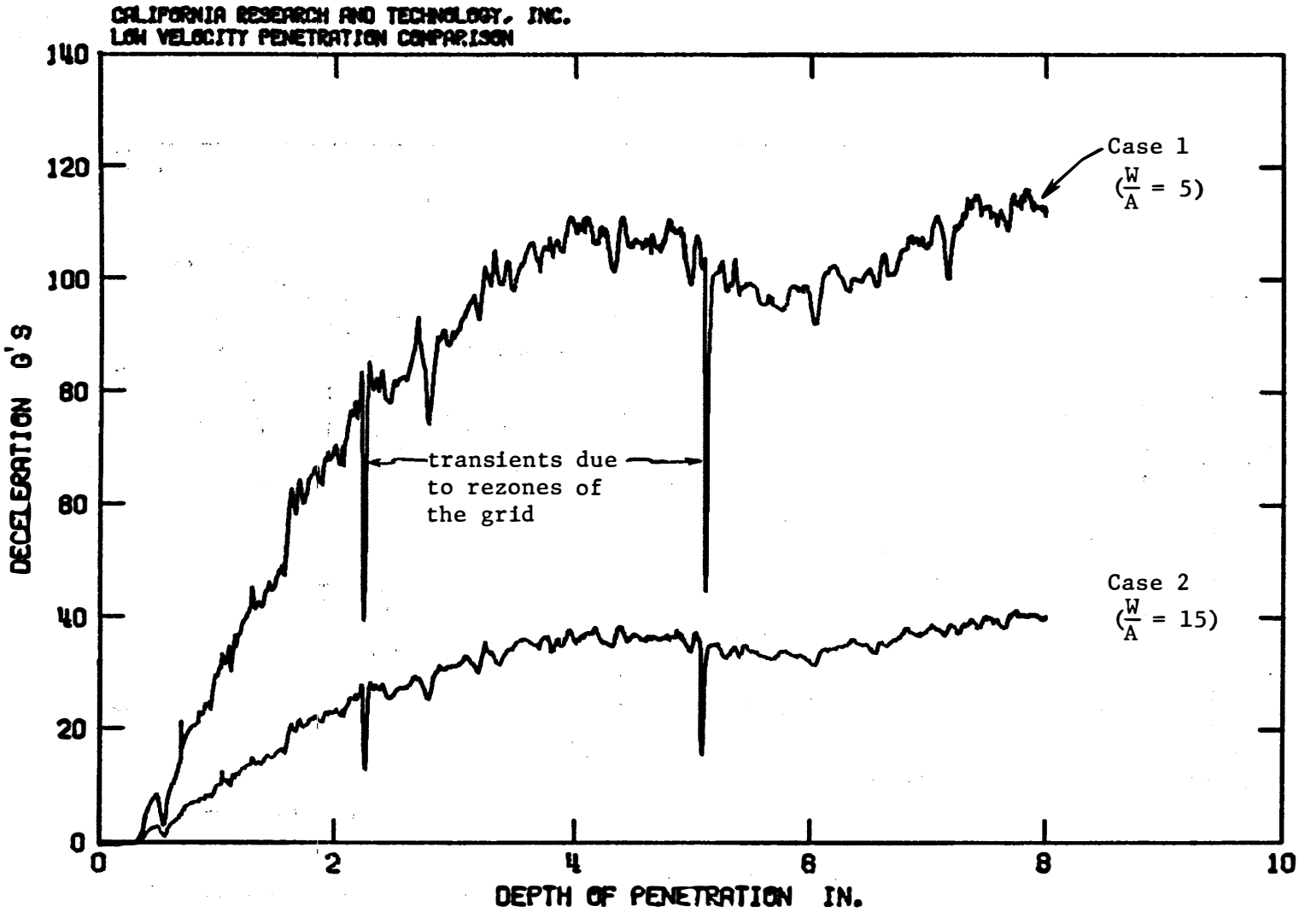

Figure 3. Penetrator Deceleration vs Depth of Penetration.

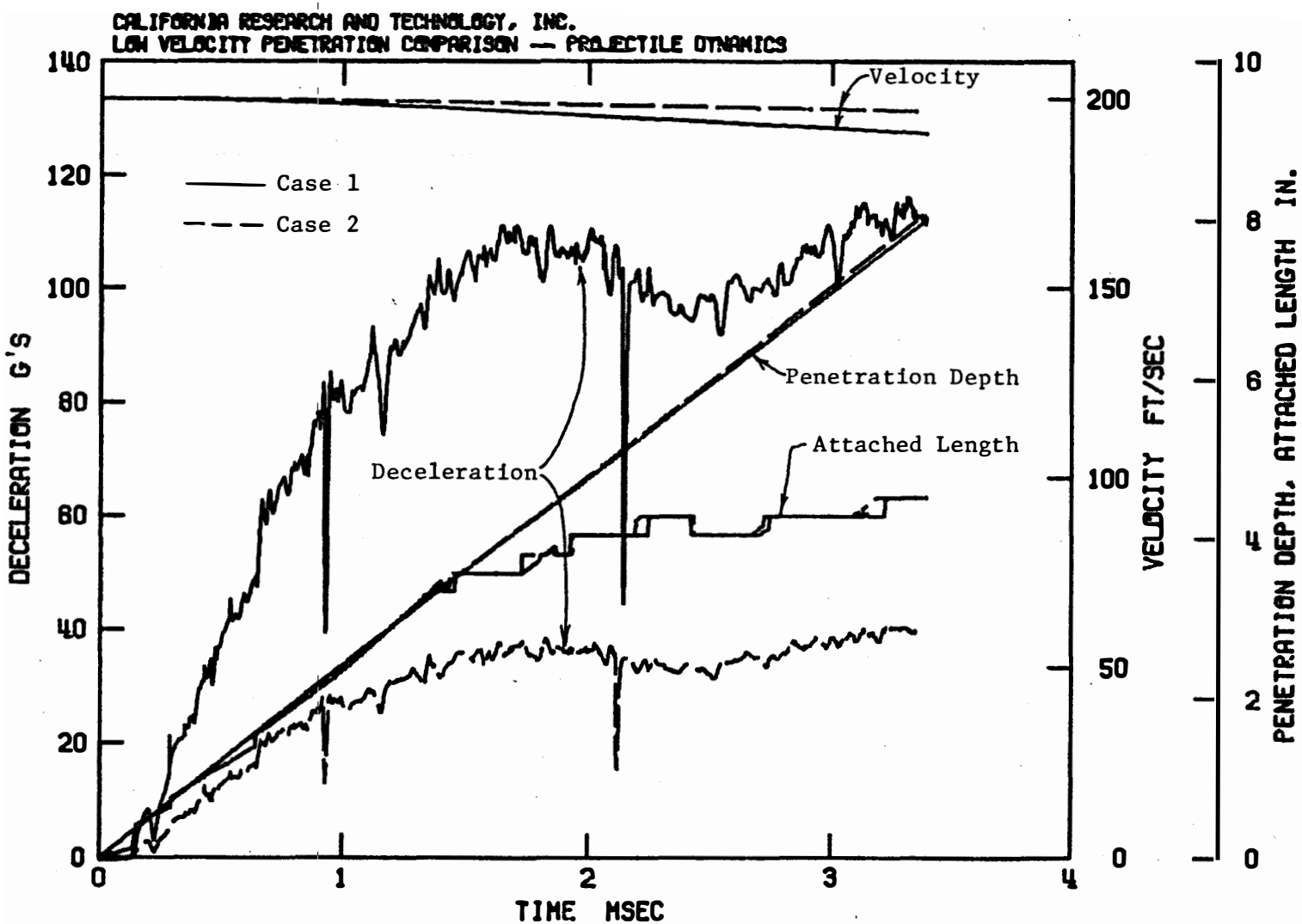

Figure 4. Time Histories of Penetrator Deceleration, Velocity, Depth of Penetration, and Attached Length.

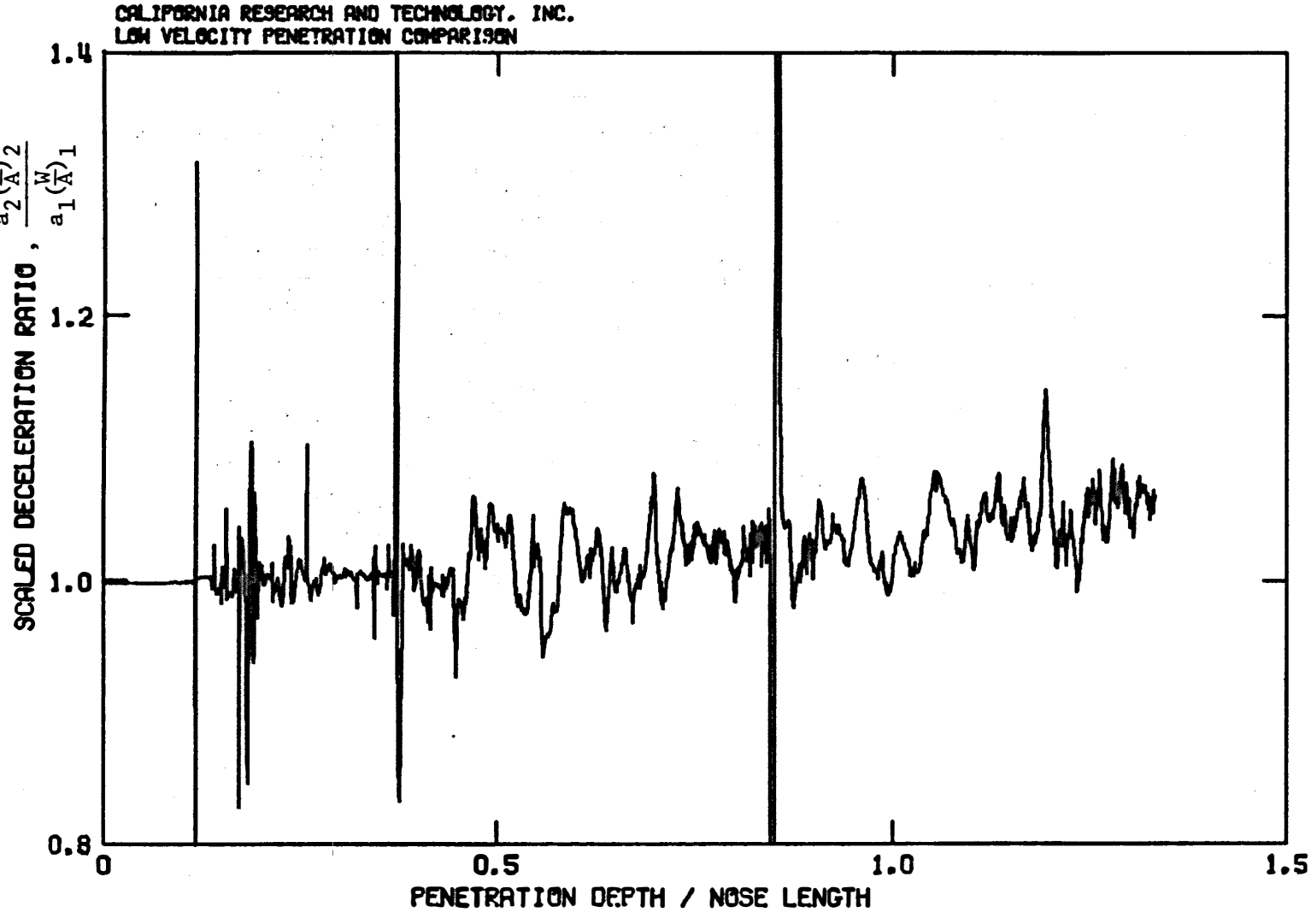

Figure 5. Ratio of Scaled Deceleration (Case 2:Case 1) vs Penetration Depth/Nose Length.

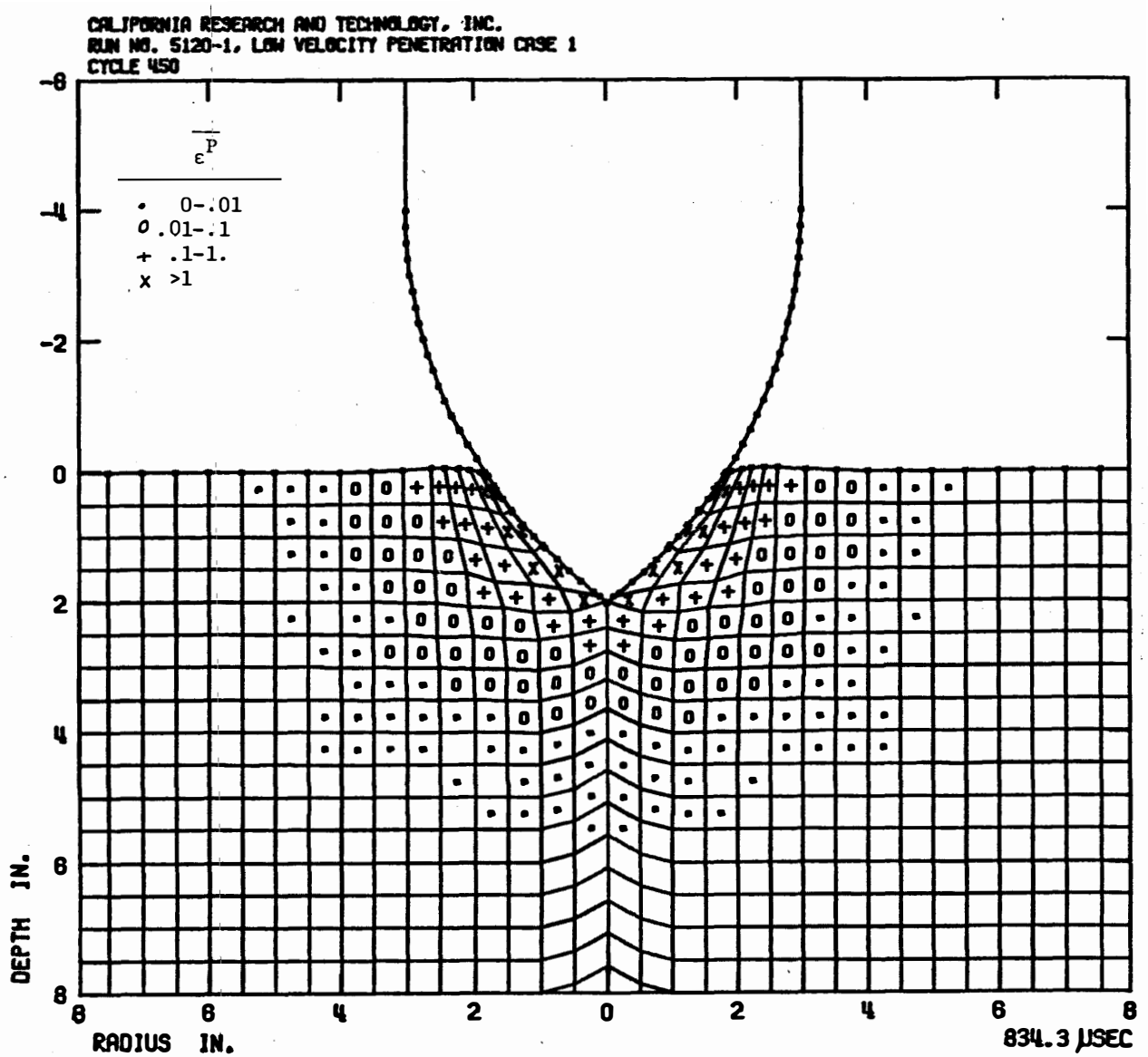

Figure 6. Grid Configuration and Generalized Plastic Strain Field at 2 in. Penetration Depth, Case 1.

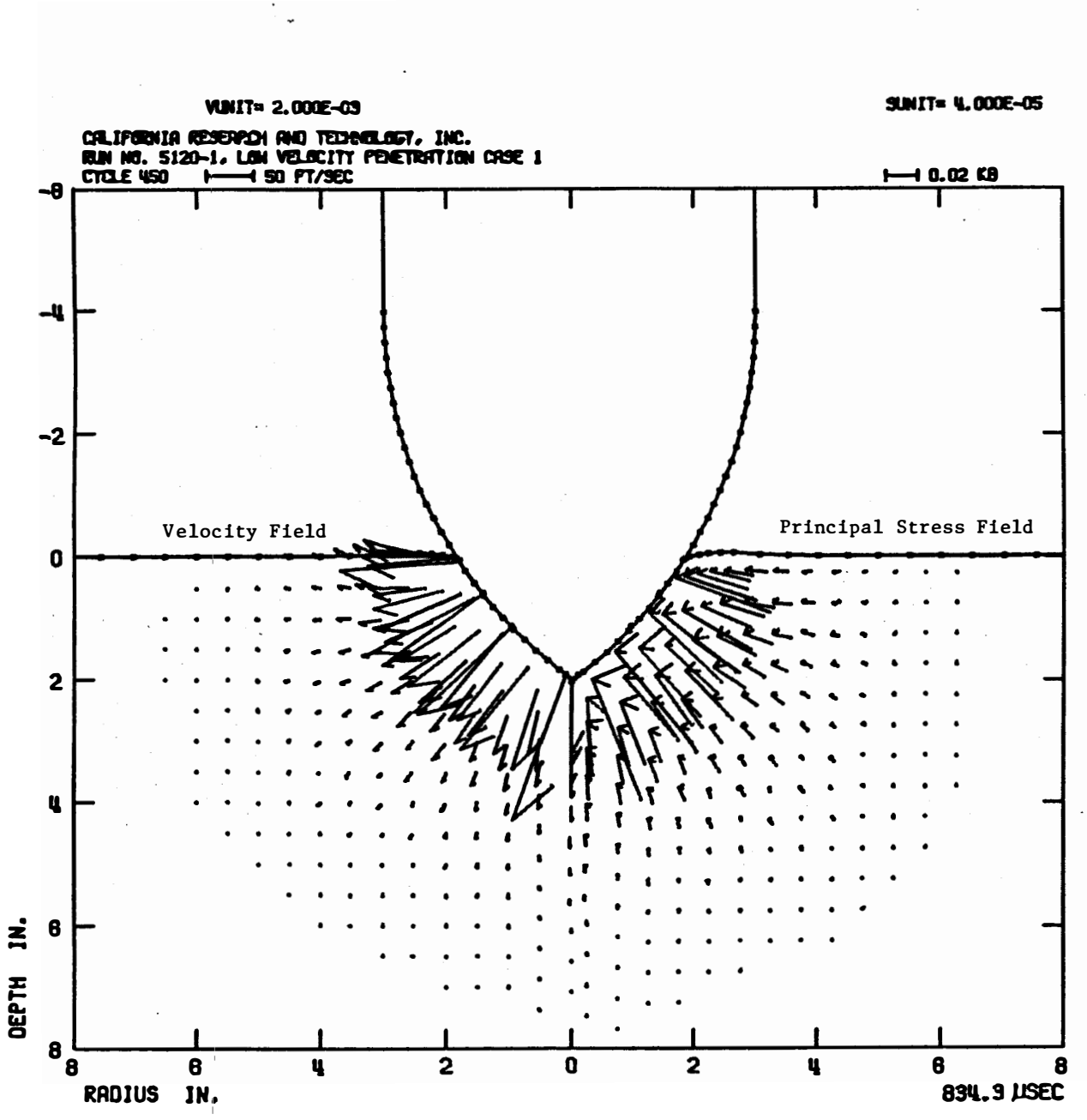

Figure 7. Velocity Field and Principal Stress Field at 2 in. Penetration Depth, Case 1.

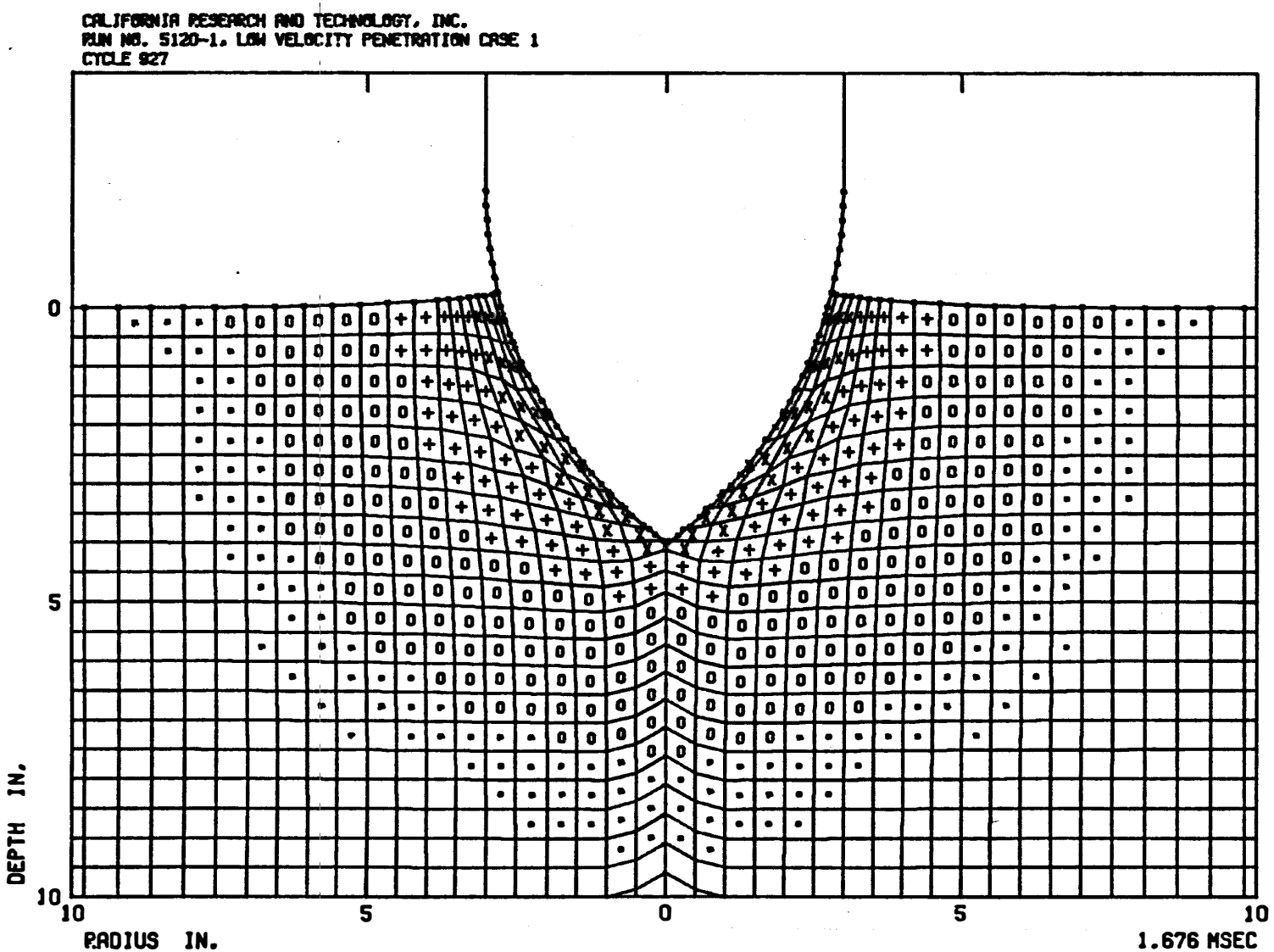

Figure 8. Grid Configuration and Generalized Plastic Strain Field at 4 in. Penetration Depth, Case 1.

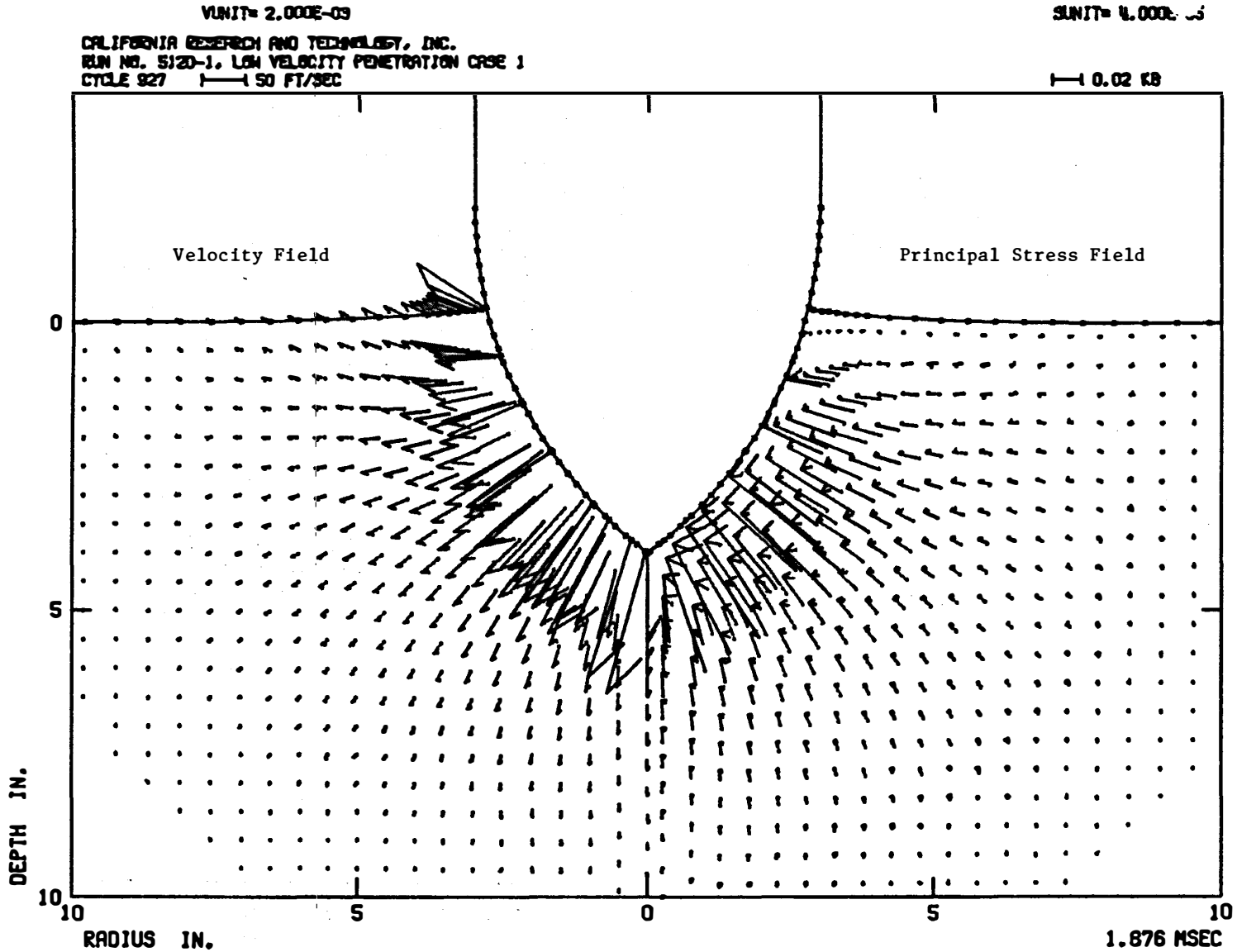

Figure 9. Velocity Field and Principal Stress Field at 4 in. Penetration Depth, Case 1.

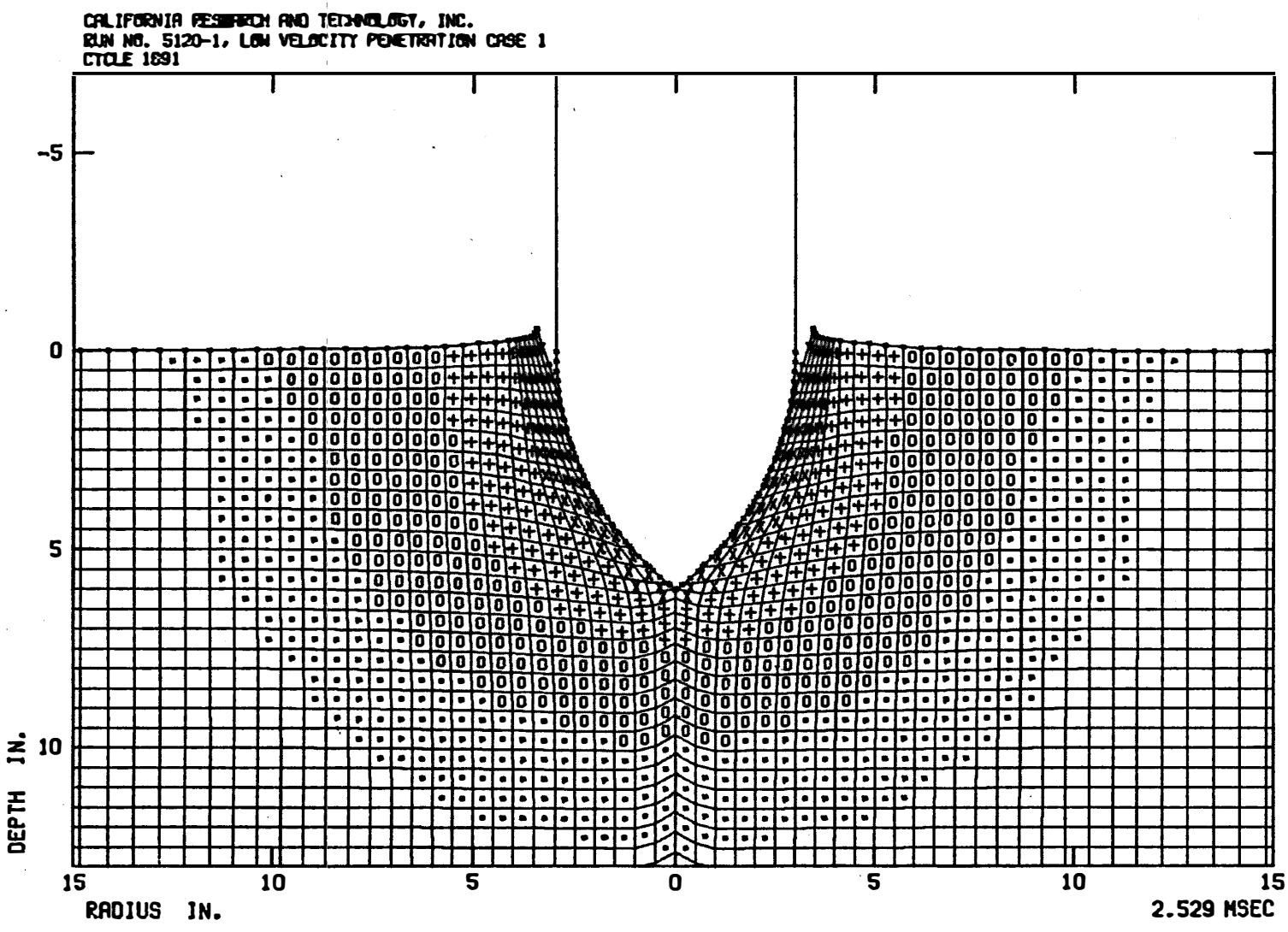

Figure 10. Grid Configuration and Generalized Plastic Strain Field at 6 in. Penetration Depth, Case 1.

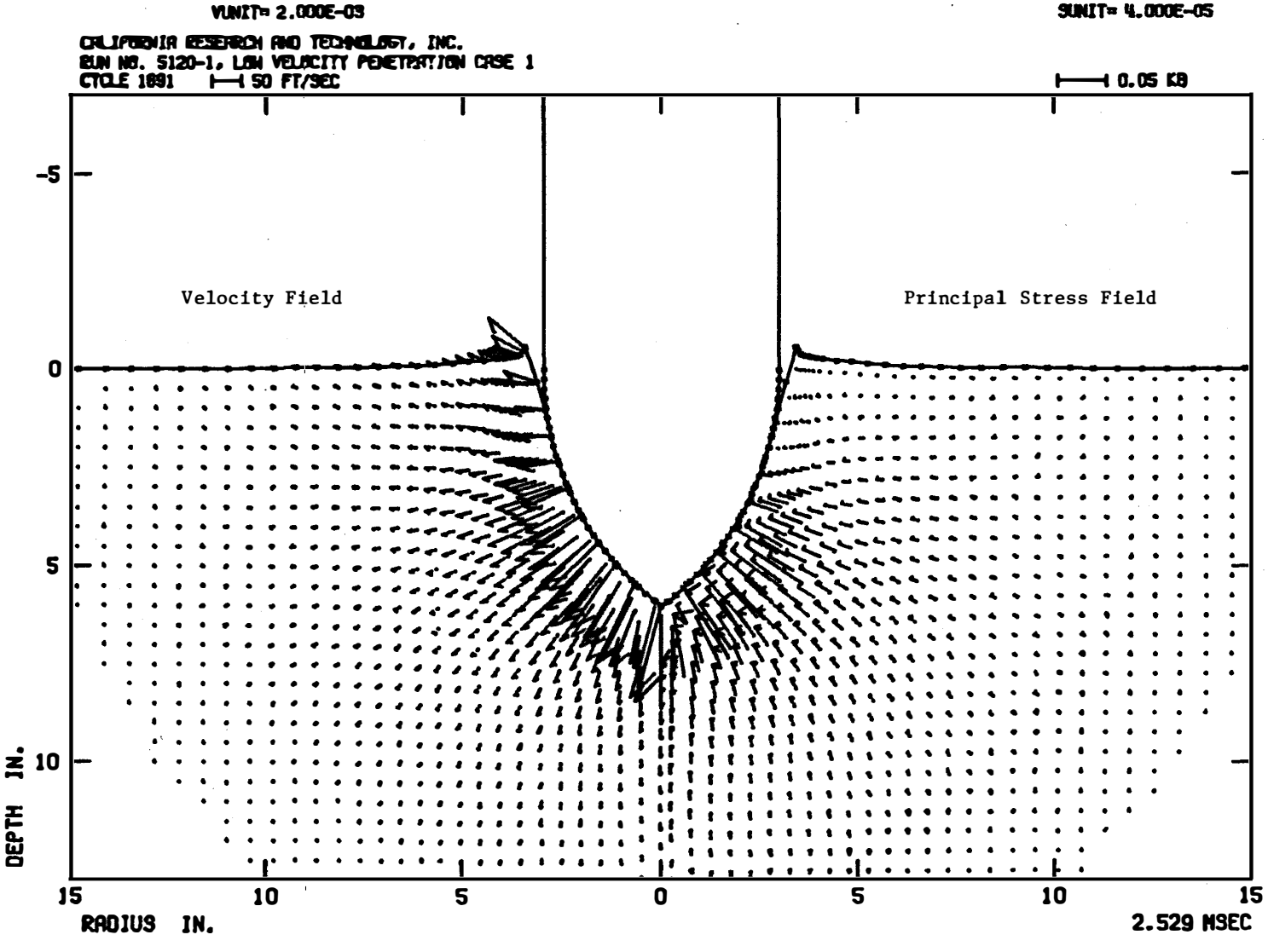

Figure 11. Velocity Field and Principal Stress Field at 6 in. Penetration Depth, Case 1.

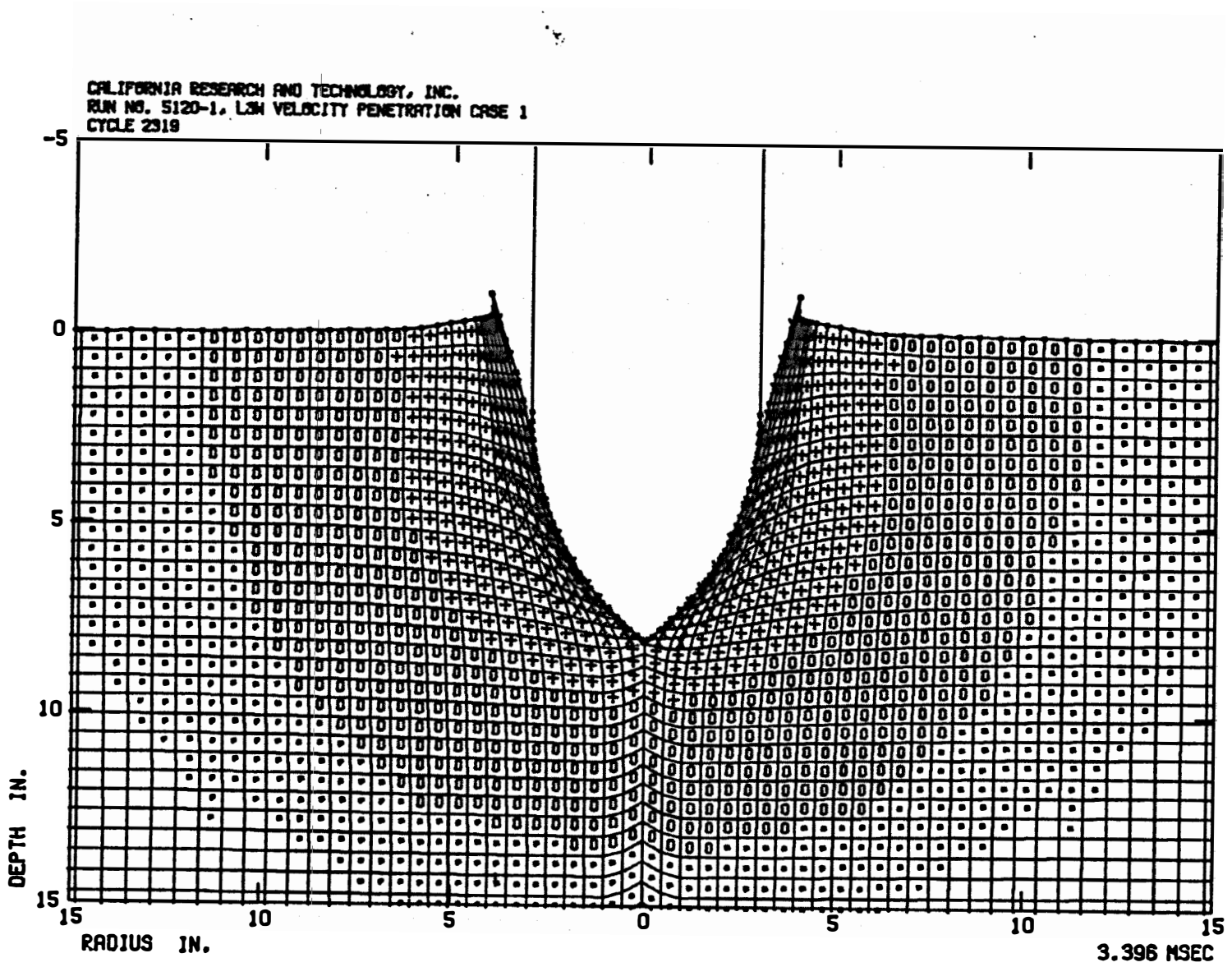

Figure 12. Grid Configuration and Generalized Plastic Strain Field at 8 in. Penetration Depth, Case 1.

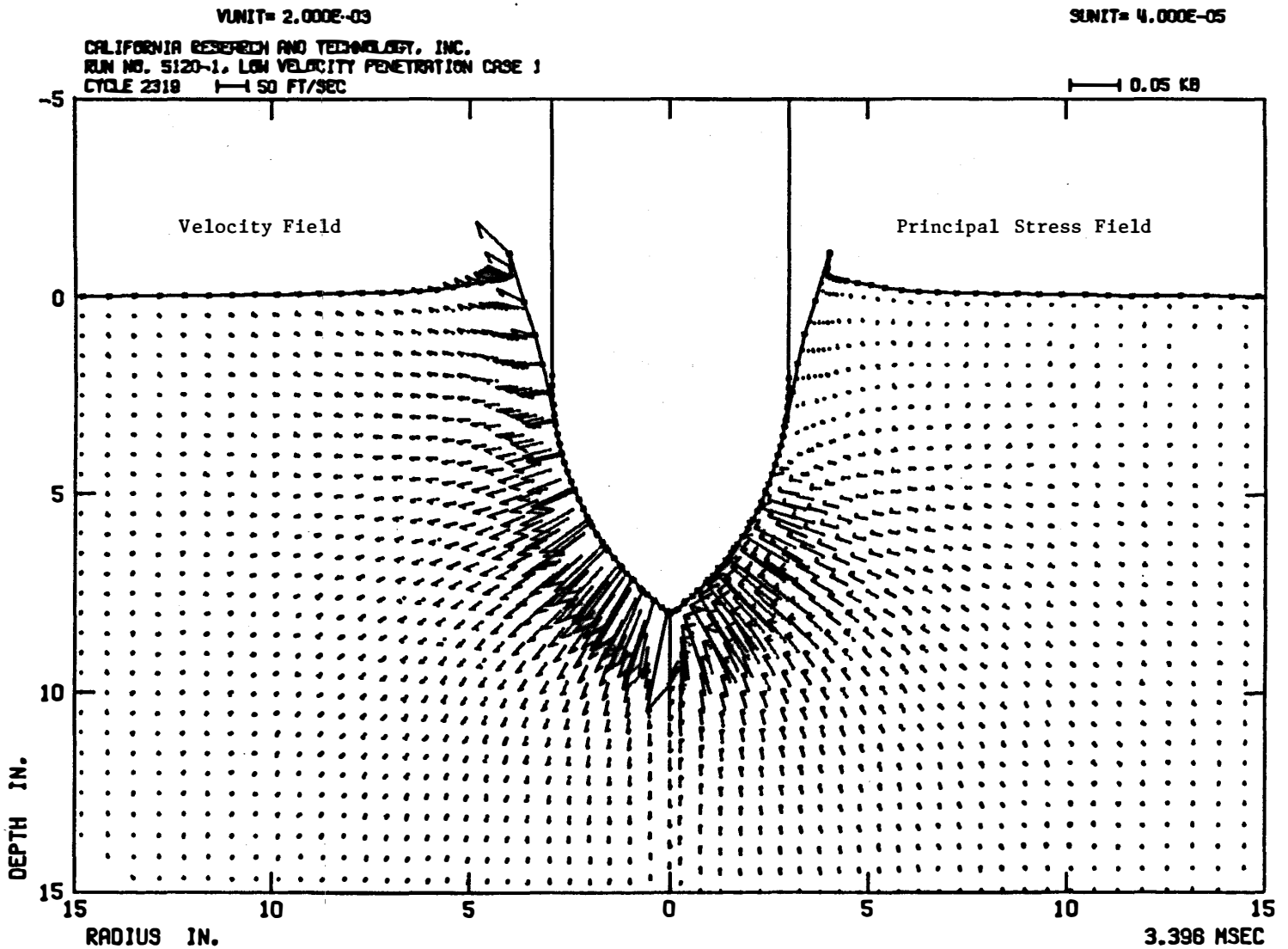

Figure 13. Velocity Field and Principal Stress Field at 8 in. Penetration Depth, Case 1.

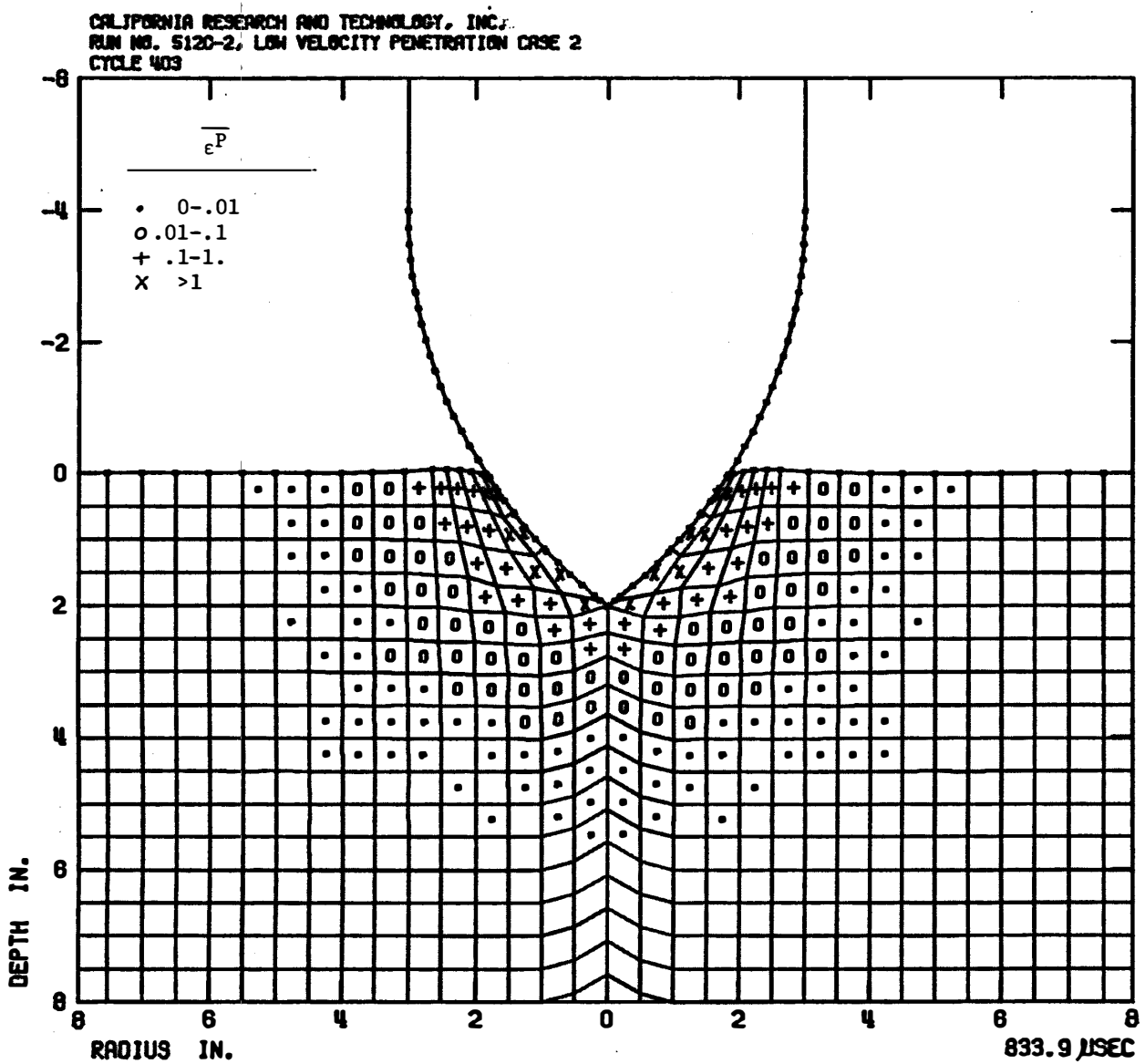

Figure 14. Grid Configuration and Generalized Plastic Strain Field at 2 in. Penetration Depth, Case 2.

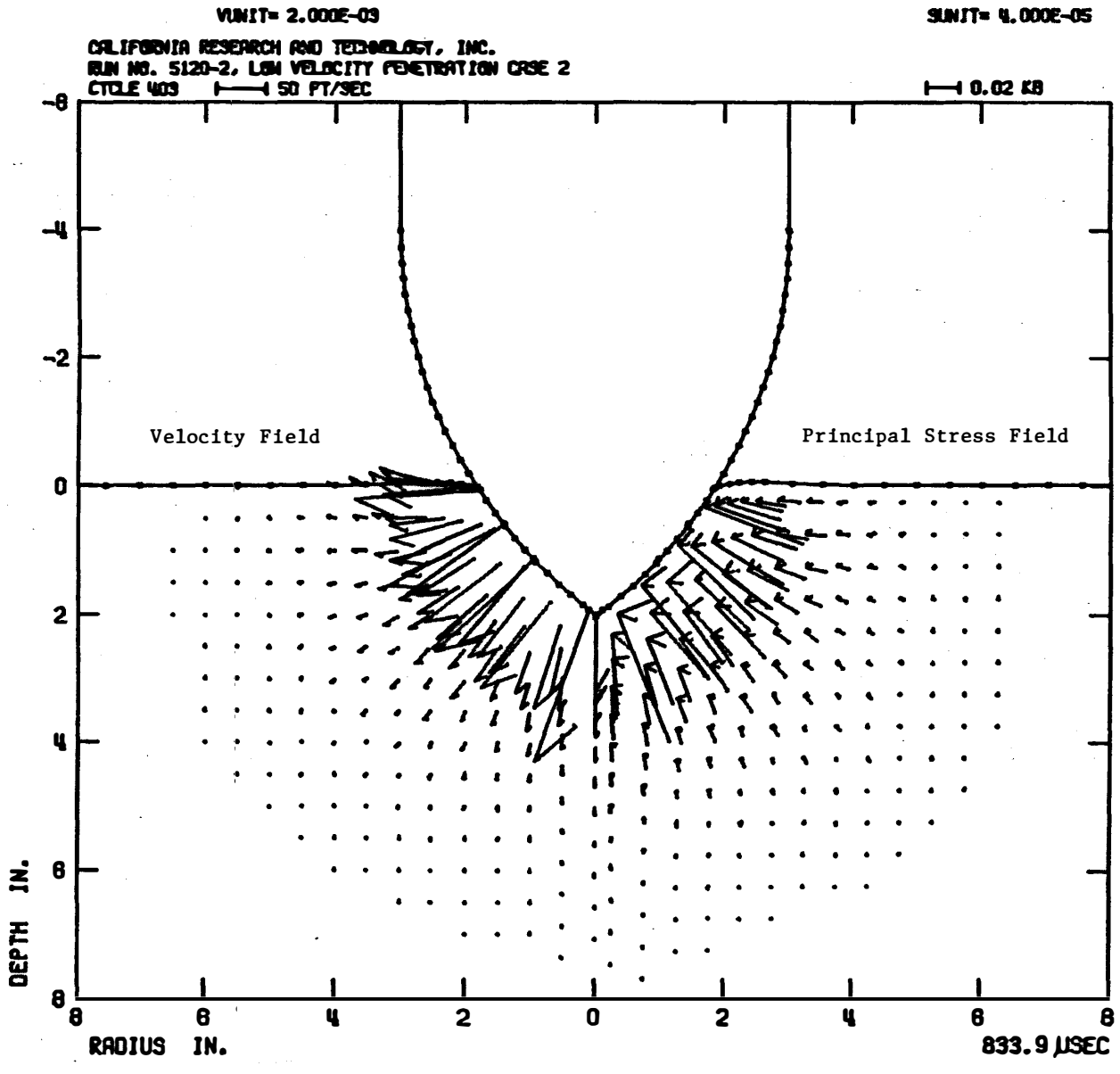

Figure 15. Velocity Field and Principal Stress Field at 2 in. Penetration Depth, Case 2.

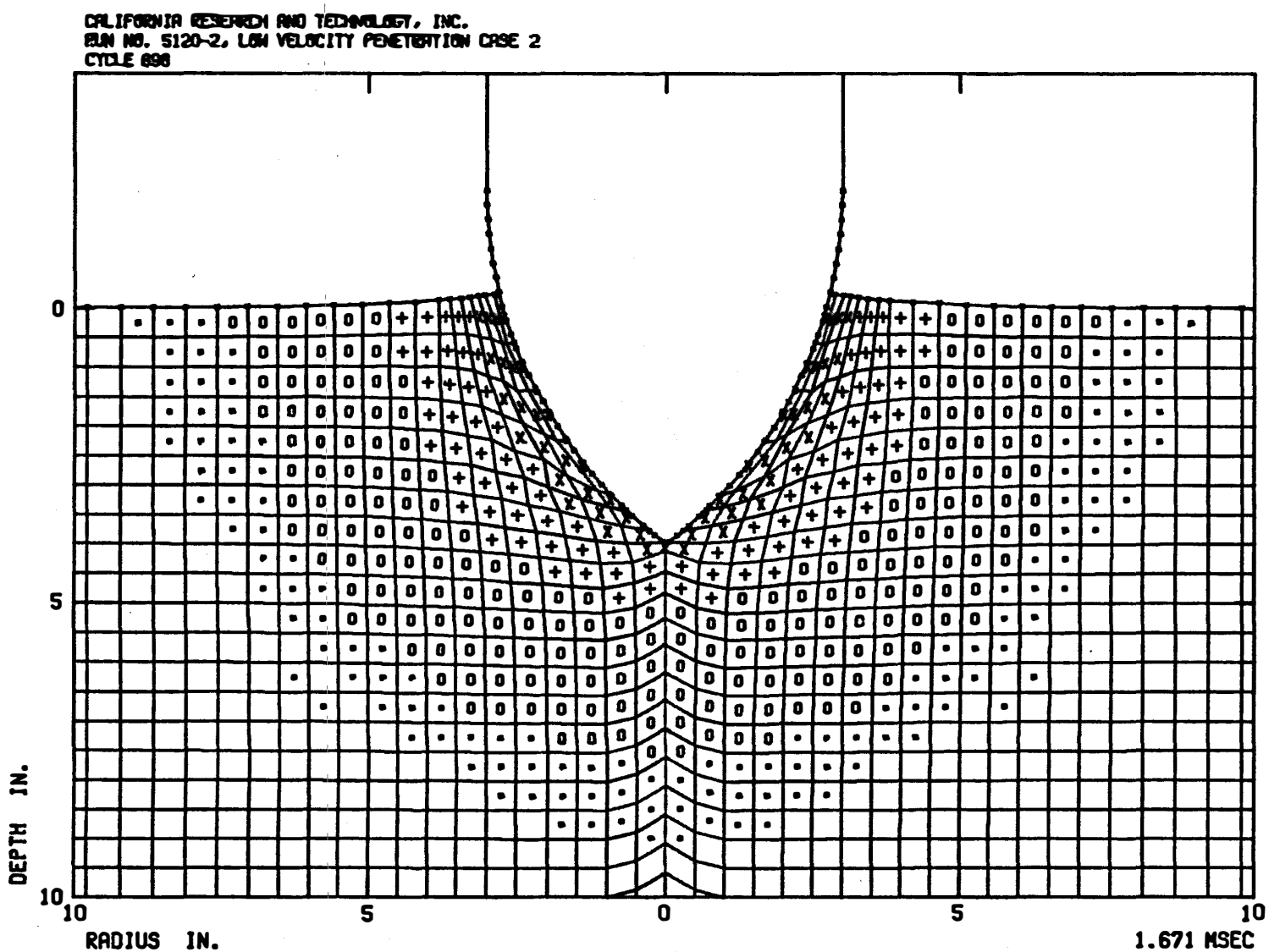

Figure 16. Grid Configuration and Generalized Plastic Strain Field at 4 in. Penetration Depth, Case 2.

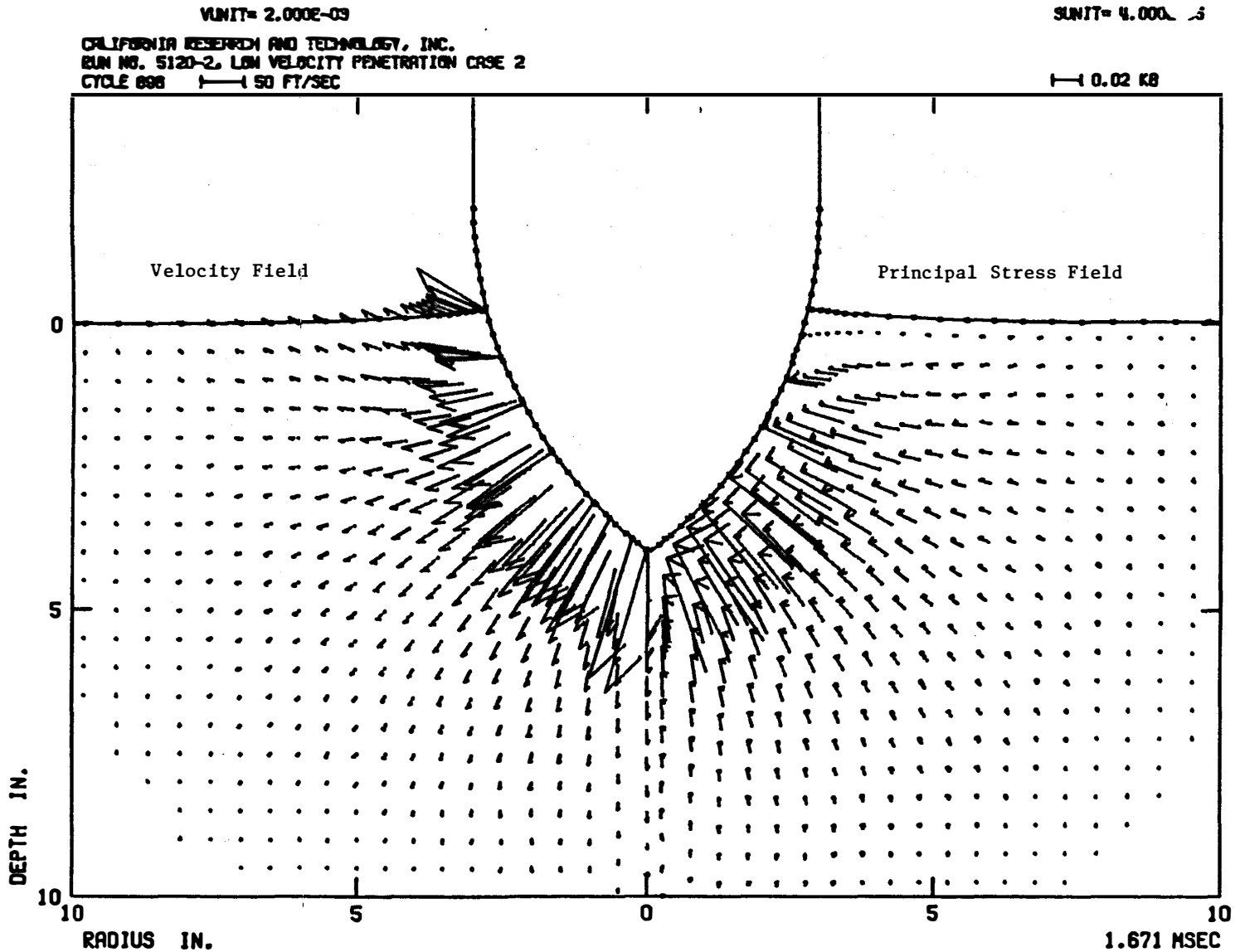

Figure 17. Velocity Field and Principal Stress Field at 4 in. Penetration Depth, Case 2.

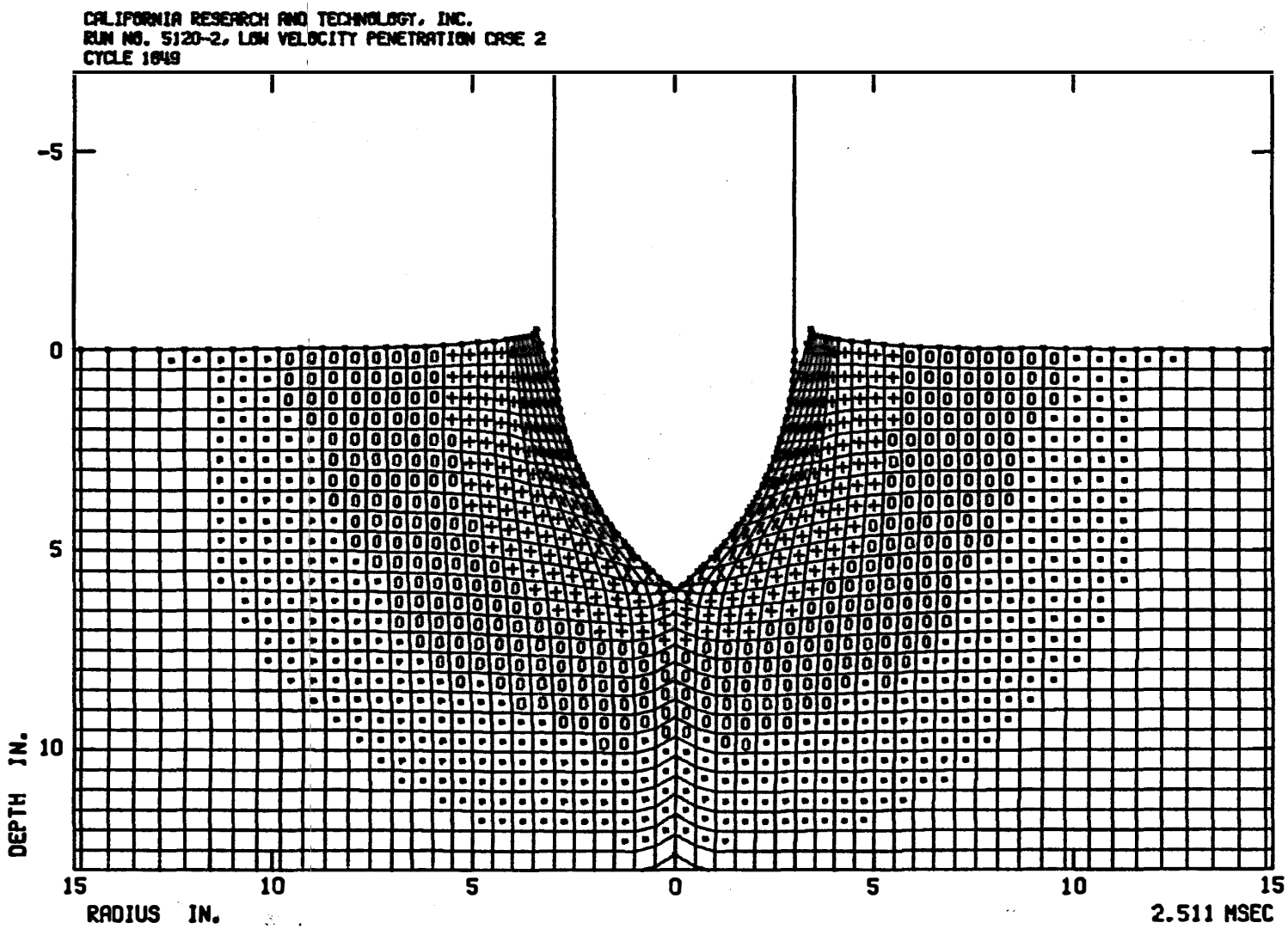

Figure 18. Grid Configuration and Generalized Plastic Strain Field at 6 in. Penetration Depth, Case 2.

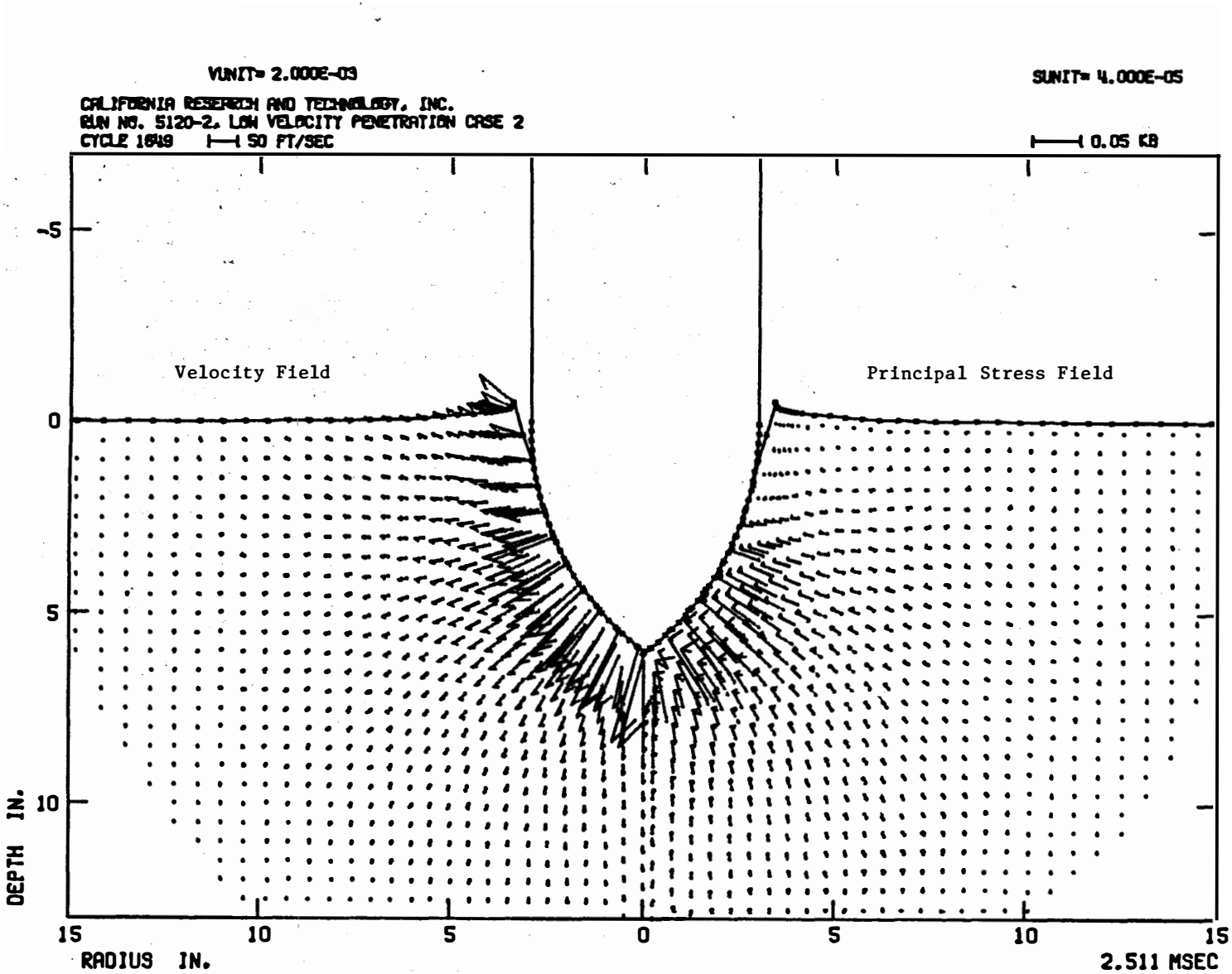

Figure 19. Velocity Field and Principal Stress Field at 6 in. Penetration Depth, Case 2.

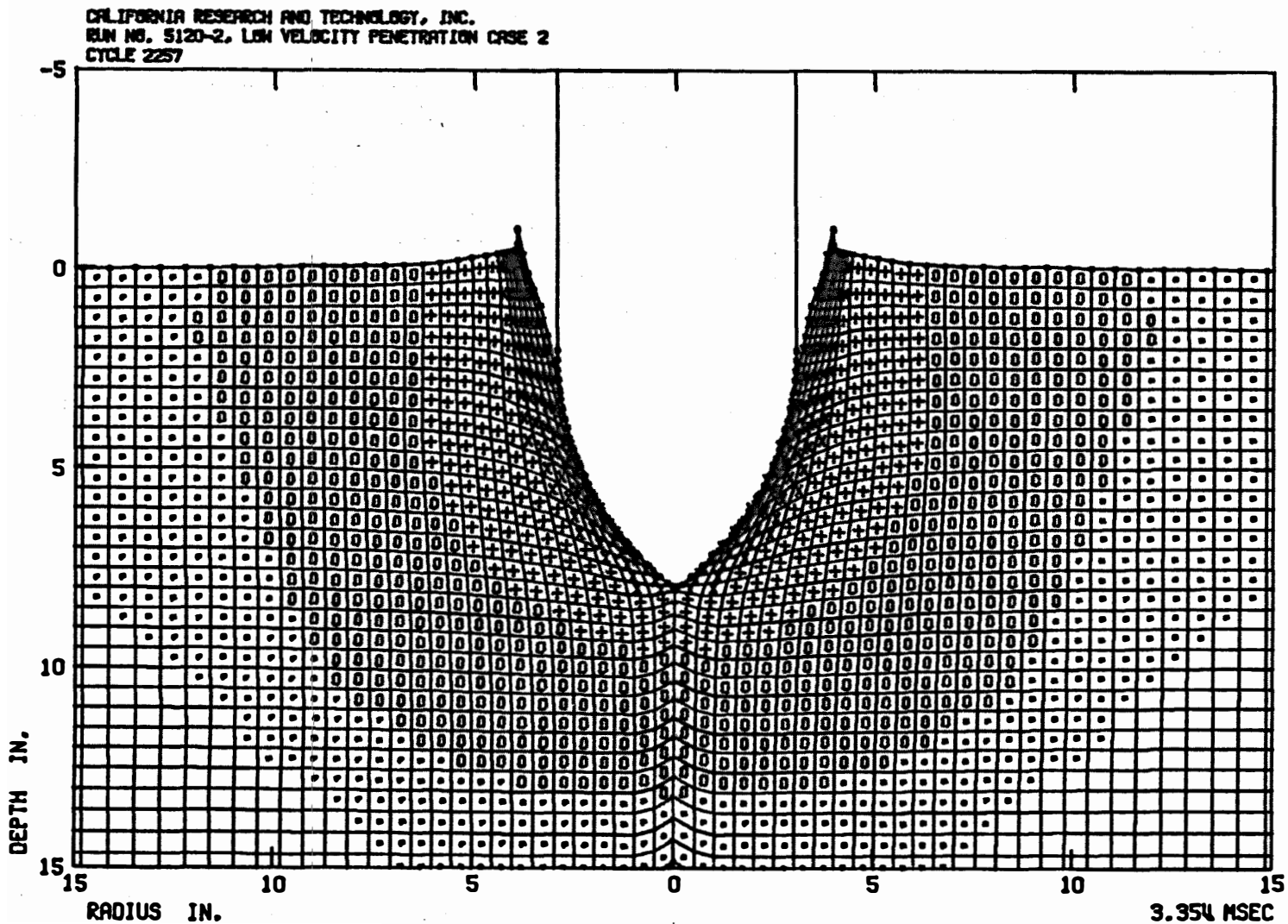

Figure 20. Grid Configuration and Generalized Plastic Strain Field at 8 in. Penetration Depth, Case 2.

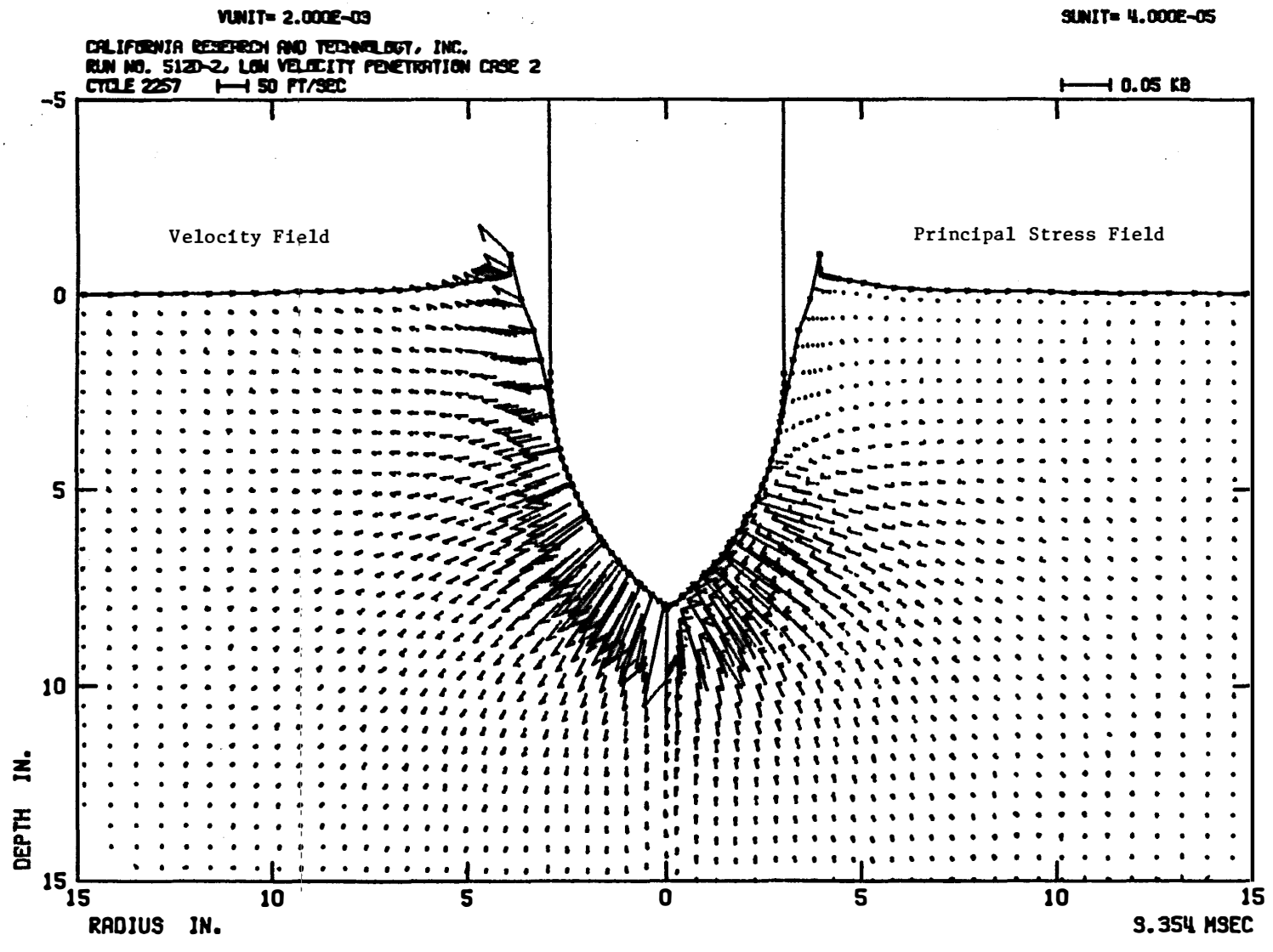

Figure 21. Velocity Field and Principal Stress Field at 8 in. Penetration Depth, Case 2.

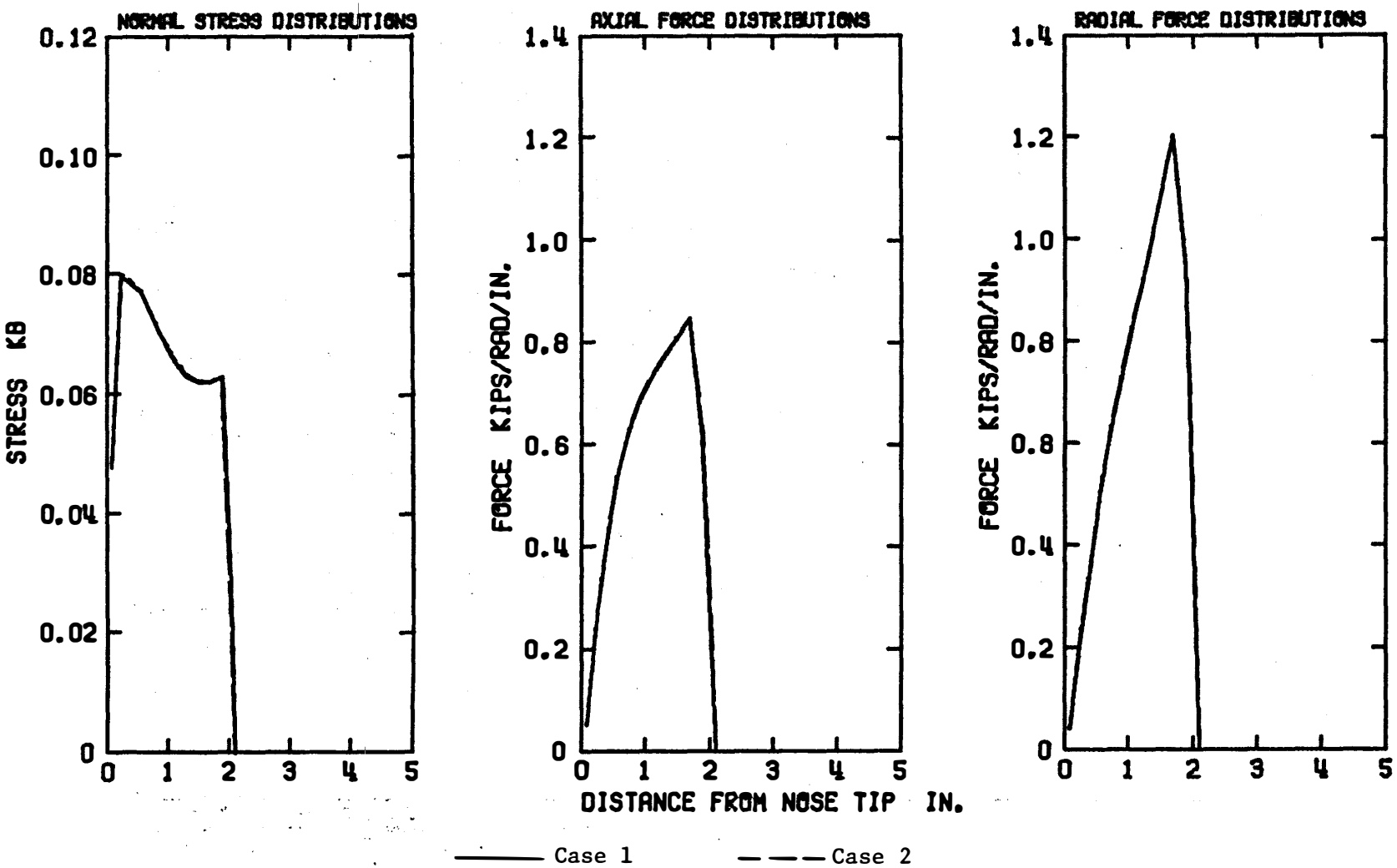

Figure 22. Penetrator Loading Distributions at 2 in. Penetration Depth.

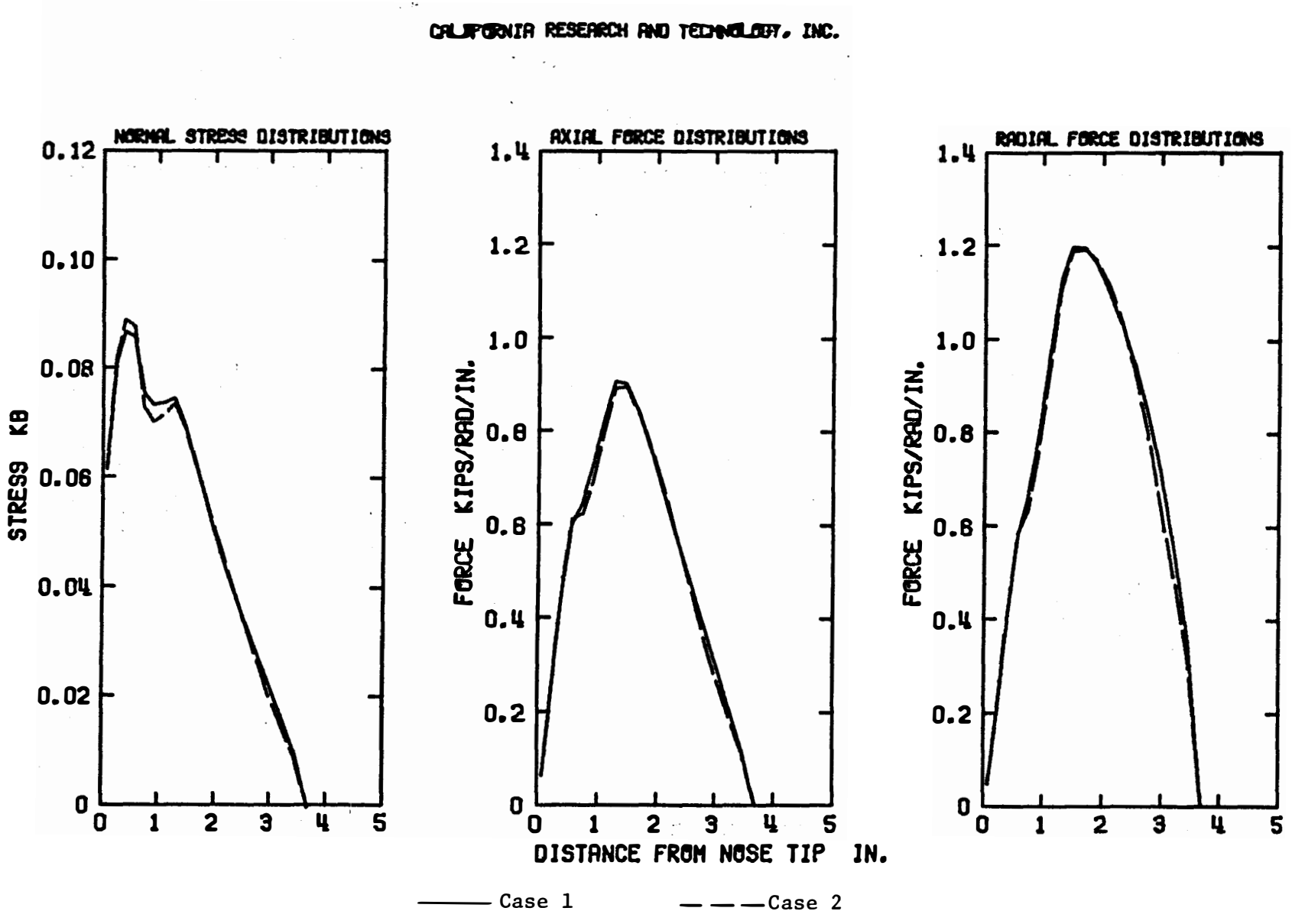

Figure 23. Penetrator Loading Distributions at 4 in. Penetration Depth.

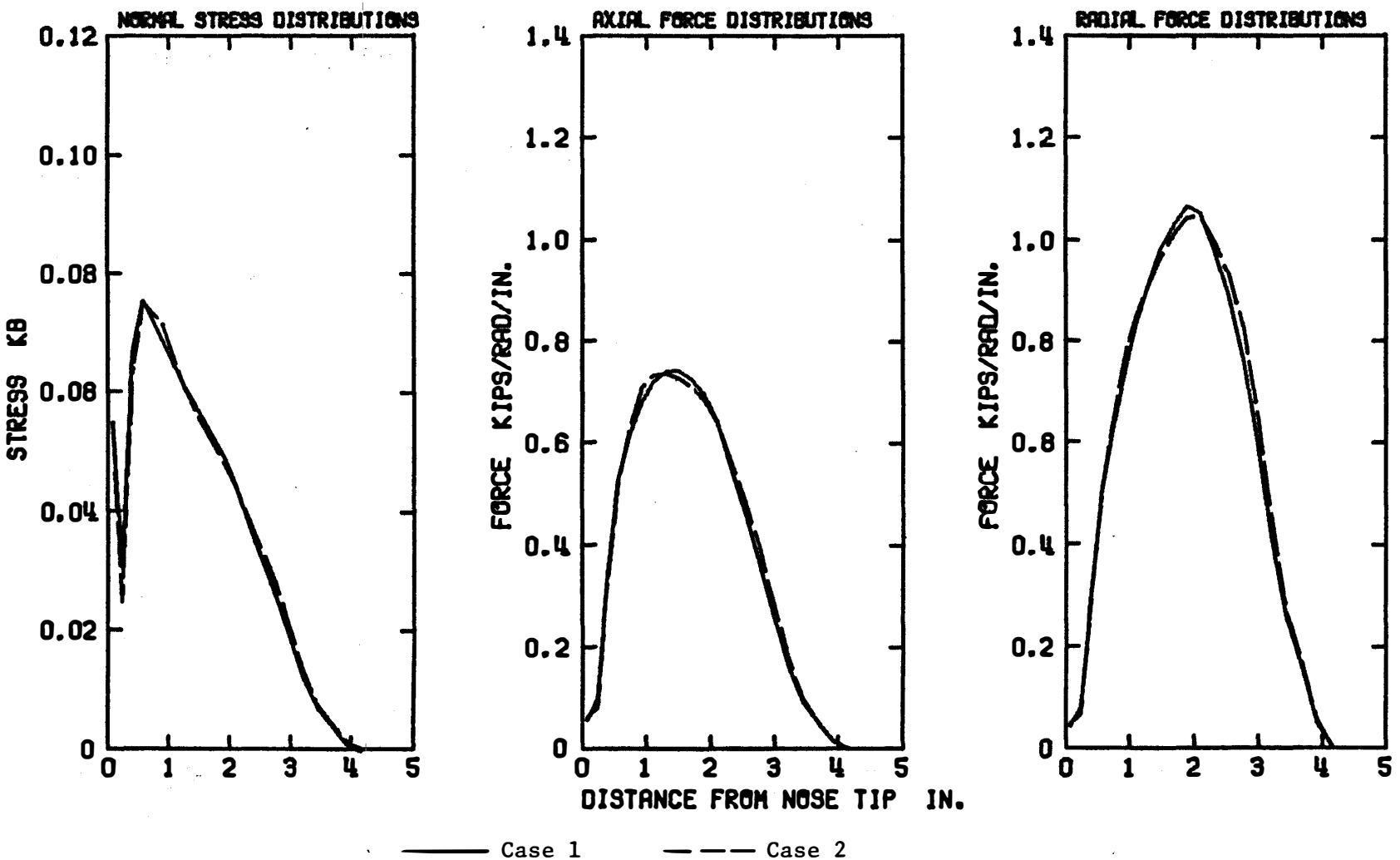

Figure 24. Penetrator Loading Distributions at 6 in. Penetration Depth.

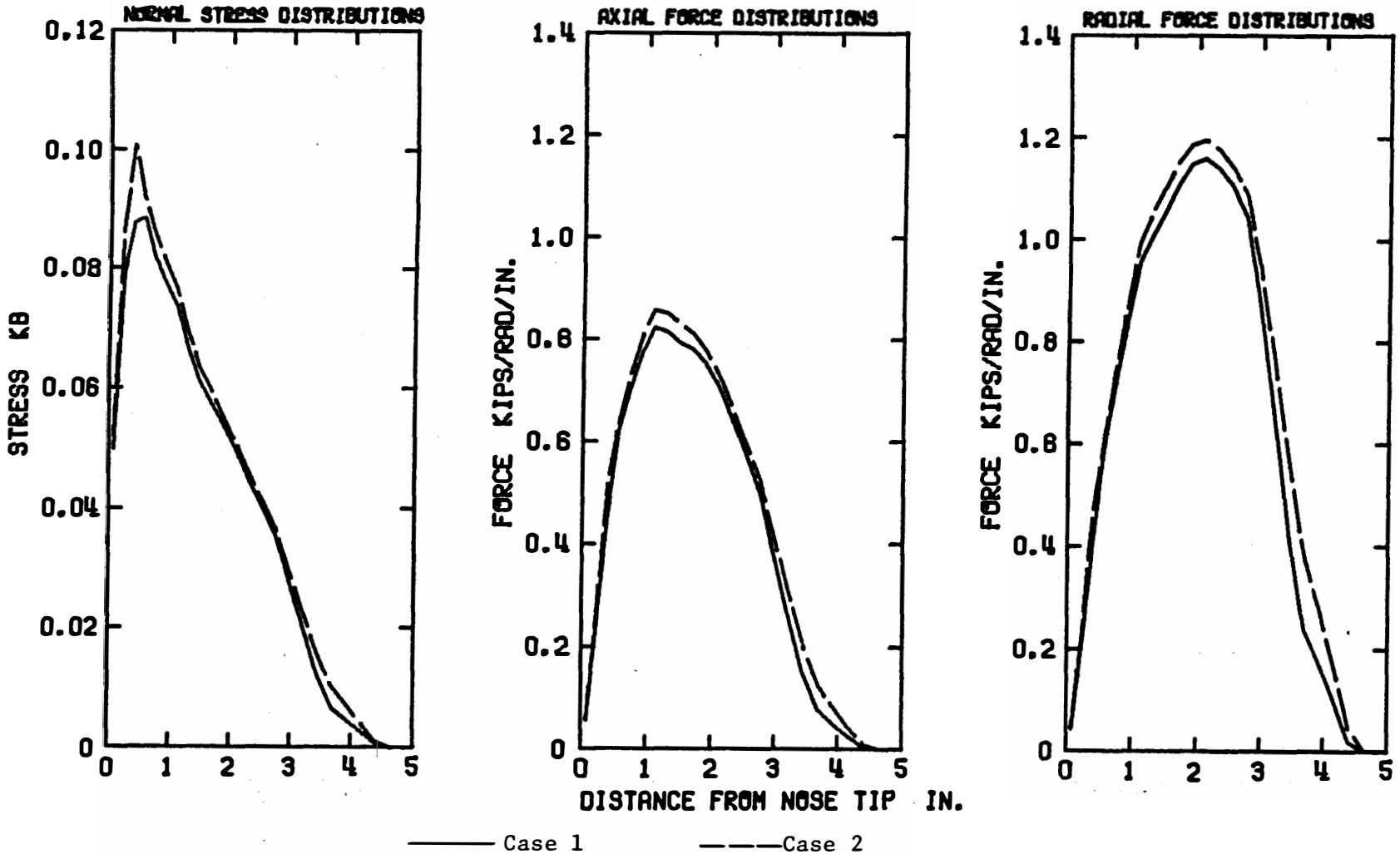

Figure 25. Penetrator Loading Distributions at 8 in. Penetration Depth.

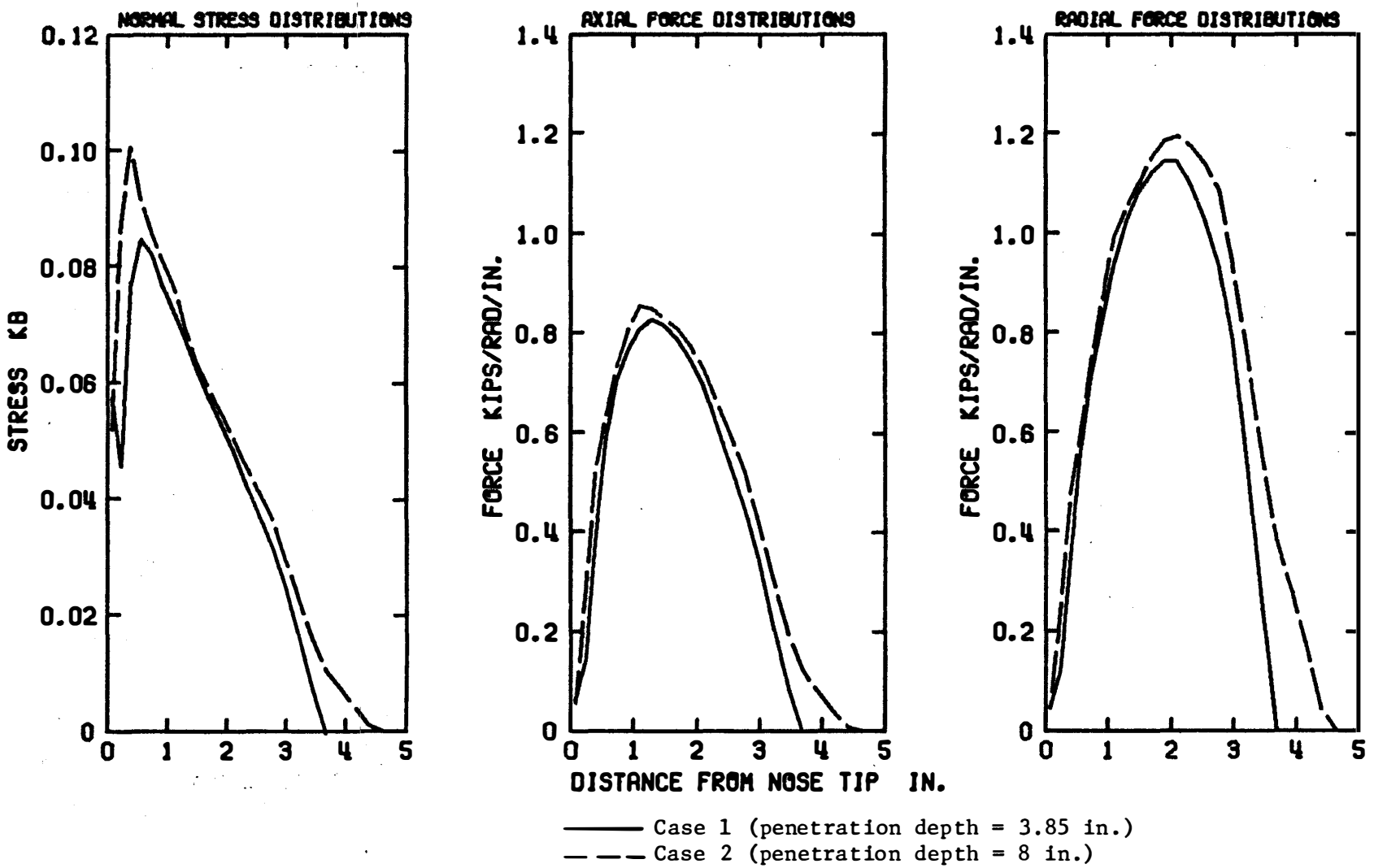

Figure 26. Penetrator Loading Distributions for Penetrator Velocity of 197 ft/sec.